NASA-CR-190692

Old Dominion University Research Foundation

!

DEPARTMENT OF MECHANICAL ENGINEERING & MECHANICS
COLLEGE OF ENGINEERING & TECHNOLOGY
OLD DOMINION UNIVERSITY
NORFOLK, VIRGINIA 23529

NAVIER-STOKES DYNAMICS AND AEROELASTIC COMPUTATIONS FOR VORTICAL FLOWS, BUFFET AND AEROELASTIC APPLICATIONS

By

Osama A. Kandil, Principal Investigator

Progress Report
For the period October 1, 1991 to September 30, 1992

September 1992

DEPARTMENT OF MECHANICAL ENGINEERING & MECHANICS
COLLEGE OF ENGINEERING & TECHNOLOGY
OLD DOMINION UNIVERSITY
NORFOLK, VIRGINIA 23529

NAVIER-STOKES DYNAMICS AND AEROELASTIC COMPUTATIONS FOR VORTICAL FLOWS, BUFFET AND AEROELASTIC APPLICATIONS
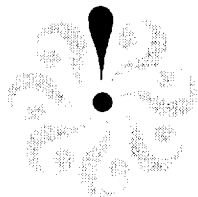
By

Osama A. Kandil, Principal Investigator

Progress Report
For the period October 1, 1991 to September 30, 1992

Prepared for
National Aeronautics and Space Administration
Langley Research Center
Hampton, VA 23665

Submitted by the
Old Dominion University Research Foundation
P.O. Box 6369
Norfolk, Virginia 23508-0369

September 1992

NAVIER-STOKES, DYNAMICS AND AEROELASTIC COMPUTATIONS FOR VORTICAL FLOWS, BUFFET AND AEROELASTIC APPLICATIONS

Osama A. Kandil[*]

Accomplishments (10/1/91–9/30/92)

The accomplishments which have been achieved on this grant in the period of 10/1/91–9/30/92 are listed. These accomplishments include conference and proceedings publications, journal papers, and abstracts which are either published, accepted for publication or under review. They also include conference presentations, NASA highlight publications and status of graduate students.

I. Conference and Proceedings Publications

The following papers have been presented at national or international conferences and have been published in conference proceedings or as refereed conference papers.

1. Kandil, O. A. and Salman, A. A., "Prediction and Control of Slender Wing Rock," International Congress of Aeronautical Sciences, ICAS Paper No. 92–4.7.2, Beijing, PRC, September 20–25, 1992 (a copy is attached).

2. Kandil, O. A. and Salman, A. A., "Three-Dimensional Simulation of Slender Delta Wing Rock and Divergence," AIAA Paper No. 92–0280, ASM, Reno, Nevada, January 6–9, f1992 (a copy is attached).

3. Kandil, O. A. and Liu, C. H., "Unsteady Vortex Flows and Flow Control Around Slender Bodies and Delta Wings," Invited Paper, Workshop on Supermaneuverability, AFOSR, Lehigh University, April 9–10, 1992, pp. 383–417.

4. Kandil, O. A. and Salman, A. H., "Recent Advances in Unsteady Computations and Applications of Vortex Dominated Flows," Invited Paper, Proceedings of the 4th International Symposium on Computational Fluid Dynamics, University of California, Davis, September 9–12, 1991, Vol. I., pp. 570–575.

5. Ph.D. Dissertation: Unsteady Euler and Navier-Stokes Computations Around Oscillating Delta Wing Including Dynamics, Department of Mechanical Engineering and Mechanics, Old Dominion University, April 1992. Advisor: Prof. Osama A. Kandil, members of committee: Drs. Woodrow Whitlow, Jr. (Head UAB) and Samuel R. Bland (UAB). Copies of the Dissertation have been delivered to Drs. Whitlow and Bland (copies of cover page, abstract and Table of Contents are attached).

---

[*] Professor and Eminent Scholar, Dept. of Mechanical Engineering and Mechanics

6. Kandil, O. A. and Salman, A. A., "Unsteady Flow Around Delta Wings with Symmetric and Asymmetric Oscillations of Leading-Edge Flaps," NAS Technical Summaries, March 1990–Feb. 1991, p. 57.

II. Journal Papers

1. Kandil, O. A. and Salman, A. A., "Unsteady Flow Around Delta Wings with Oscillating Leading-Edge Flaps," Accepted for Publication in the Journal of Aircraft, to appear in August 1993.

2. Kandil, O. A., Salman, A. A. and Chuang, H. A., "Unsteady Flow Computations of Oscillating Flexible Wings," Accepted for Publication in the Journal of Aircraft, to appear in August 1993.

3. Kandil, O. A. and Salman, A. A., "Computational Simulation and Flaps Active Control of Delta Wing Rock," Accepted for Publication in the AIAA Journal, to appear in September 1993.

III. Talks and Presentations

1. Kandil, O. A., "Recent Advances in Unsteady Computations and Applications of Vortex Dominated Flows," International Symposium on Computational Fluid Dynamics, University of California, Davis, September 9–12, 1991.

2. Kandil, O. A., "Three-Dimensional Simulation of Slender Delta Wing Rock and Divergence," Aerospace Sciences Meeting, Reno, Nevada, January 6–9, 1992.

3. Kandil, O. A., "Unsteady Vortex Flows and Flow Control Around Slender Bodies and Delta Wings," Workshop on Supermaneuverability, AFOSR, Lehigh University, April 9–10, 1992.

4. Salman, A. A., "Unsteady Euler and Navier-Stokes Computations Around Oscillating Delta Wing Including Dynamics," Ph.D. Dissertation Defense, MEM Dept., Old Dominion University, April 1992.

5. Kandil, O. A., "Unsteady Vortex Flows and Flow Control Around Slender Bodies and Delta Wings," Canadian Air Force Group, Unsteady Aerodynamics Branch, May 14, 1992. A Simulation movie has been shown for 3 flow solutions (a copy is delivered to Dr. Whitlow).

6. Kandil, O. A., "Prediction and Control of Slender Wing Rock," International Congress of Aeronautical Sciences, Beijing, PRC, September 20–25, 1992.

IV. Graduate Students

– **Dr. Ahmed A. Salman:** finished his Ph.D. dissertation in May 1992. He spent three months as a Research Associate, and he is leaving on August 21, 1992 to Egypt where he is appointed as an assistant professor, Faculty of Engineering, Zagazig University, Egypt.

– **Mr. Mark Flanagan (US Citizen):** Started his M.S. program in September 1991. He was supported through the MEM Department from September 1991–May 1992. Currently, he is supported through the present grant. He started working on his M.S. thesis in January 1992 and his effort is directed toward the quasiaxisymmetric tail-buffet model in a configured duct. He is expected to finish his M.S. thesis in March 1993. He will be staying for his Ph.D. degree. His Ph.D. research work will focus on a generic model for three-dimensional tail-buffet problem where combined bending and torsion modes are considered along with its control.

– **Mr. Steven Massey (US Citizen):** Started his M.S. program in January 1992. He will start working on his M.S. thesis as of September 1992. His effort will be directed toward the three-dimensional tail-buffet problem in an unbound domain consisting of a delta wing followed by a vertical tail. He will be supported from the present grant as of October 1992.

– **Mrs. Tahani Amer (US Citizen):** She is finishing her B.S. project under the Virginia Space Grant in December 1992. She is staying for her M.S. degree and will be supported under this grant. Her effort will be directed toward active control using leading-edge injection of the wing rock motion.

AIAA-92-0280

THREE-DIMENSIONAL SIMULATION OF SLENDER DELTA WING ROCK AND DIVERGENCE

Osama A. Kandil and Ahmed A. Salman

Old Dominion University, Norfolk, VA 23529

30th Aerospace Sciences Meeting & Exhibit
January 6-9, 1992 / Reno, NV

THREE-DIMENSIONAL SIMULATION OF SLENDER DELTA WING ROCK AND DIVERGENCE

Osama A. Kandil* and Ahmed A. Salman**
Old Dominion University, Norfolk, VA 23529

Abstract

Computational simulation of three-dimensional flows around a delta wing undergoing rock and roll-divergence motions is presented. The problem is a multidisciplinary one where fluid-dynamics equations and rigid-body-dynamics equations are sequentially solved. For the fluid-dynamics part, the unsteady Euler equations, which are written relative to a moving frame of reference, are solved using an implicit, approximately-factored, central-difference, finite-volume scheme. For the rigid-body-dynamics part, the Euler equation of rigid-body rolling motion is solved using a four-stage Runge-Kutta scheme. Since the applications do not include deforming wings or relative-rigid-body motions, the computational-fluid-dynamics grid, which is fixed in the moving frame of reference, does not need to be updated once it is generated.

Introduction

The dynamic phenomenon of wing rock is characterized by large-amplitude, high-frequency, rolling oscillation with a limit-cycle amplitude. The rolling oscillation is self excited and it is triggered by vortex-flow asymmetry or vortex breakdown on highly swept delta wings at high angles of attack. The study of this phenomenon is vital for the dynamic stability and controllability of high performance aircraft during maneuvering and landing.

Several experimental investigations[1-6] have been conducted to gain basic understanding of the phenomenon. Nguyen, et al.[1] tested a flat-plate delta wing with 80° leading-edge sweep for forced-oscillation, rotary and free-to-roll tests. The free-to-roll tests showed that the wing exhibited a rock motion at angles of attack greater than 25°, and that the rock motion reached the same limit-cycle condition independent of the initial conditions. Levin and Katz[2] tested two delta wings with leading-edge sweeps of 76° and 80°. They found that only the wing with the 80° sweep would undergo a rock motion. Nelson and his co-workers[3,4,6] have conducted a series of experimental studies to investigate the mechanisms responsible for wing rock on a delta wing with 80° leading-edge sweep. Their analysis revealed that the primary mechanism for the phenomenon was a time lag in the position of the vortices normal to the wing surface. Moreover, they concluded, through the analysis of separate contributions of

the wing upper and lower surface-pressure distributions, that the upper surface pressure provides all of the instability and little damping in the roll moment and that the lower surface pressure provides the classical roll damping hysteresis. Morris and Ward[5] conducted dynamic measurements in both a water tunnel and a wind tunnel on a delta wing with leading-edge sweep of 80°. Their results showed that the measured hysteresis loops in the water tunnel were opposite in direction from those of the wind tunnel. They concluded that the hysteresis direction does not play as decisive a role as previously thought in initiating and sustaining wing rock.

Erickson[7,8] analyzed experimental data for aircraft configurations at high angles of attack in an attempt to reveal the flow processes which generate wing rock. He concluded that wing rock phenomenon for slender wings is caused by asymmetric-leading-edge vortices and that the vortex breakdown provides a limiter to the growth of wing-rock amplitude. He also identified another two mechanisms for limit-cycle oscillations in roll of advanced aircraft.

The literature review showed that numerical simulation of this phenomenon for low speeds has recently been presented by Konstadinopoulos, et al.[9]. This has been followed by developments of analytical models to investigate the parameters affecting this phenomenon. Nayfeh, et al.[10-11] have presented two analytical models and Hsu and Lan[12] have presented one analytical model. The improved analytical model of Nayfeh, et al.[11] proved to be superior in comparison with the Hsu and Lan model and more accurate than their first model of reference[10]. The model of reference[11] accurately fitted the rolling moment coefficient, which was computed by a vortex-lattice method, using five terms which included the linear aerodynamic damping and restoring moments and the nonlinear aerodynamic damping moments. With this model, it was shown on the phase plane that both the wing rock and wing-roll divergence were possible responses for the wing. Hsu and Lan's model cannot predict wing-roll divergence. A serious question which can be raised regarding the work in references 9-12 is: how accurate the fluid dynamics solution is, using the vortex lattice method? Moreover, the fluid dynamics model limits its applicability to low-speed flows and to angles of attack below the critical value for vortex breakdown. Moreover, the

---

*Professor and Eminent Scholar, Dept. of Mechanical Engineering and Mechanics, Associate Fellow AIAA
**Research Assistant, Same Dept., Member AIAA

1

vortex lattice model also cannot predict separated flows from smooth surfaces.

The first computational unsteady solution for the forced-rolling oscillation of a delta wing, which was based on the unsteady Euler equations, was presented by Kandil and Chuang[13]. The solution used the locally-conical flow assumption for supersonic flows in order to reduce the computational time by an order of magnitude as compared to that of the three-dimensional solutions. Forced-pitching oscillation of airfoils were also considered in a later paper by Kandil and Chuang[14]. The first unsteady three-dimensional Euler solution for the forced-pitching oscillation of a delta wing was also presented by Kandil and Chuang[15]. The unsteady Navier-Stokes solutions were also used by Kandil and Chuang[16] for the forced-rolling oscillation of a delta wing under the locally-conical flow assumption. Batina[17] developed a conical Euler solver, which was based on the use of un-structured grids, and used it to solve for the flow around a delta wing undergoing forced-rolling oscillation under the locally-conical flow assumption. Later on, Lee and Batina[18] extended the Euler solver to include a free-to-roll capability to solve for a freely rolling delta wing which exhibited wing rock. The solution was based on the locally-conical flow assumption. In Ref. 19, the present authors studied symmetric and anti-symmetric forced-rolling oscillations of the leading-edge flaps of a delta wing. A hinge is considered at the 75% location of the local half span and the leading-edge flaps are forced to oscillate both symmetrically and anti-symmetrically. The Navier-Stokes and Euler equations are used to solve the problem along with the Navier-displacement equation to account for the grid deformation due to the leading-edge flaps motion. In a later paper by the authors[20], the effects of symmetric and anti-symmetric flaps oscillation with varying frequencies have been investigated for two flow conditions. With the aid of these studies, the authors[21,22] studied the wing rock phenomenon as well as its active control using anti-symmetric tuned oscillations of the wing leading-edge flaps. The sequential solutions of unsteady Euler equations and the Navier-displacement equations along with the Euler equation of rigid-body rolling motion were used to obtain the solutions for these problems. The locally-conical flow assumption was also used throughout these solutions.

In this paper, we present the first three-dimensional computational simulation using the Euler equations for flows around a delta wing undergoing wing-rock and roll-divergence motions. The solutions are obtained using the sequential solutions of the Euler equations for fluid flows and the Euler equations for rigid-body rolling motion. The equations and the boundary conditions are written with respect to a moving frame of reference. Since no active control through the leading-edge flaps oscillations is used in this paper, there is no need to move the computational grid once it is generated the first time.

Formulation

The formulation of the problem consists of two sets of equations. The first set is the unsteady Euler equations which are written relative to a moving frame of reference. This set is used to compute the flowfield for steady or unsteady flows. The second set is the Euler equations of rigid-body rolling motion. This set is used to compute the wing motion when the dynamics problem is coupled with the fluid dynamics problem.

Unsteady Euler Equations For Flowfield

Using the transformation equations from the space-fixed frame of reference to a moving frame of reference (Refs. 13-16), the non-dimensional, unsteady, Euler equations are transformed to the moving frame of reference. Such a transformation eliminates the need to move the computational grid for rigid wings having time-dependent rigid-body motion. Hence, the Euler equations are given by

$$\frac{\partial \bar{Q}}{\partial t} + \frac{\partial \bar{E}_m}{\partial \xi^m} = \bar{S} \tag{1}$$

where

$$\bar{Q} \equiv \text{flowfield vector} = \frac{\hat{q}}{J} = \frac{1}{J}[\rho, \rho u_1, \rho u_2, \rho u_3, \rho e]^t \tag{2}$$

$$\xi^m = \xi^m(x_1, x_2, x_3) \tag{3}$$

$$\begin{aligned} \bar{E}_m \equiv \text{inviscid flux} &= \frac{1}{J}\left(\partial_k \xi^m \hat{E}_k\right) \\ &= \frac{1}{J}[\rho U_m, \rho u_1 U_m + \partial_1 \xi^m p, \rho u_2 U_m \\ &+ \partial_2 \xi^m p, \rho u_3 U_m + \partial_3 \xi^m p, \rho U_m h]^t \end{aligned} \tag{4}$$

$$U_m = \partial_k \xi^m u_k \tag{5}$$

$$\bar{S} \equiv \text{source term due to rigid–body motion} = \frac{1}{J}\hat{S}$$

$$\begin{aligned} &= \frac{1}{J}\{0, -\rho(a_t)_1, -\rho(a_t)_2, -\rho(a_t)_3, -\rho[\bar{V} \cdot \bar{a}_o \\ &+ (\bar{\omega}x\bar{r}) \cdot \bar{a}_o + \bar{V}_o \cdot (\bar{a}_t - \bar{\omega}x\bar{V}) + \bar{V} \cdot (\dot{\bar{\omega}}x\bar{r}) \\ &+ (\bar{\omega}x\bar{r}) \cdot (\dot{\bar{\omega}}x\bar{r})]\}^t \end{aligned} \tag{6}$$

$$\bar{V} = \bar{V}_a - \bar{V}_t \equiv \text{relative velocity} \tag{7}$$

$$\bar{V}_t = \bar{V}_o + \bar{\omega}x\bar{r} \tag{8}$$

$$\bar{a}_t = \bar{a}_o + \dot{\bar{\omega}}x\bar{r} + 2\bar{\omega}x\bar{V}_o + \bar{\omega}x(\bar{\omega}x\bar{r}) \tag{9}$$

$$p = \rho(\gamma - 1)\left(e - \frac{V^2}{2} + \frac{V_t^2}{2}\right) \tag{10}$$

$$h = \frac{\gamma p}{\rho(\gamma - 1)} + \frac{V^2}{2} - \frac{V_t^2}{2} \qquad (11)$$

The reference parameters for the dimensionless form of the equations are $L, a_\infty, L/a_\infty$ and ρ_∞ for the length, velocity, time and density, respectively. In Eqs. (1)-(11), ρ is the density, u_n the relative fluid velocity component, $\bar{V}_o$ and $\bar{a}_o$ translation velocity and acceleration of the moving frame, $\bar{V}_t$ and $\bar{a}_t$ the transformation velocity and acceleration from the space-fixed to the moving frames of reference, $\bar{\omega}$ and $\dot{\bar{\omega}}$ the angular velocity and acceleration of the moving frame, L the wing chord length, $\bar{r}$ the fluid position vector, p the pressure, e and h the total energy and enthalpy per unit mass relative to the moving frame and γ the gas index which is set equal to 1.4.

Euler Equation For Rigid-Wing Rolling Motion

Here, we consider a rigid wing fixed on an axle which rotates in bearings. The bearing damping coefficient is λ. Torsional springs of stiffness k are assumed at the ends of the axle. If I_{xx} is the mass-moment of inertia of the wing around the axle and if M_x is the aerodynamic rolling moment around the axle, then the governing equation of motion is given by

$$M_x = I_{xx}\ddot{\theta} + \lambda\dot{\theta} + k\theta \qquad (12)$$

where θ is the roll angle which is positive in the counter-clockwise direction.

Computational Schemes

The computational scheme used to solve Eqs. (1)-(11) is an implicit, approximately-factored, centrally-differenced, finite-volume scheme[13-15]. Added second-order and fourth-order explicit dissipation terms are used in the difference equation on its right-hand side terms, which represent the explicit part of the scheme. The Jacobian matrices of the implicit operator on the left-hand side of the difference equation are centrally-differenced in space, and implicit second-order dissipation terms are added for the scheme stability. The left-hand side spatial operator is approximately factored and the difference equation is solved in three sweeps in the ξ^1, ξ^2 and ξ^3 directions, respectively.

For the wing-rock problem, Eq. (12) is solved using a four-stage Runge-Kutta scheme. Starting from known initial conditions for θ and $\dot{\theta}$, the equation is explicitly integrated in time in sequence with the fluid dynamics equations, Eqs. (1-11). Equation (12) is used to solve for θ, $\dot{\theta}$ and $\ddot{\theta}$ while Eqs. (1-11) are used to solve for M_x. If the initial M_x is nonzero, a case of asymmetric steady flow at initial conditions, the initial values of θ and $\dot{\theta}$ are set equal to zero and the motion is initiated by the initial rolling moment.

Computational Applications and Discussion

A sharp-edged delta wing with a leading-edge sweep of 80° is considered for the computational applications. The angle of attack is set at 30° and the freestream Mach number is chosen as 0.3 for low speed simulation. The wing mass-moment of inertia about its axis is 0.285, the bearings damping coefficient is 0.15 and the torsional springs stiffness is 0.74. The unsteady Euler equations are solved for the three-dimensional flows. The boundary of the computational domain consists of a hemispherical surface with it center at the wing trailing edge on its line of geometric symmetry. The hemispherical surface is connected to a cylindrical aftersurface with its axis coinciding with the wing axis. The hemispherical and cylindrical radii are two root-chord lengths and the downstream, circular exit boundary is at two root-chord lengths from the wing trailing edge. The grid consists of 32×32×48 grid points in the axial, normal and wrap-around directions, respectively. The grid is generated in the crossflow planes using a modified Joukowski transformation, which is applied at the grid-chord stations with exponential clustering at the wing surface.

Steady Flow (Initial Conditions)

Figure 1 shows the results for the steady flow at $\alpha = 30°$ and $M_\infty = 0.3$. The results include the crossflow-velocity vectors and static-pressure contours at three-chord stations of 0.54, 0.79 and 0.91; and the surface-pressure coefficient at two chord stations of 0.54 and 0.79. The results show that although the wing is at zero sideslip angle, the flow is asymmetric. The primary vortex on the right side produces more suction pressure than the one on the left side, and hence there is a net counter-clockwise (CCW) rolling moment. Using these results for the initial conditions of the wing-rock problem, the wing is released from rest at zero roll angle ($\theta_o = 0$) and zero roll velocity ($\dot{\theta}_o = 0$).

Simulation of Wing Rock

Since the steady flow solution is asymmetric, M_x in Eq. (12) is of non-zero value and hence Eq. (12) is initially inhomogeneous. At $t = 0$, we set $\theta_o = \dot{\theta}_o = 0$ and release the wing with its initial M_x value as the driving rolling moment. At $t = \Delta t$, Eq. (12) of the wing dynamics is integrated to obtain θ and hence $\dot{\theta}$ and $\ddot{\theta}$ ($\Delta t = 0.005$). Then, Eqs. (1-11) of the fluid flow are integrated to obtain the components of the flowfield vector and hence p and M_x. Next, t is increased to $2\Delta t$ and the sequential integration of the dynamics equation and the fluid flow equations is repeated. The sequential solutions are repeated until the limit-cycle amplitude response is reached

In Fig. 2, we show in the first row the roll angle, rolling-moment coefficient, M_x, and normal-force coefficient, C_N, versus time, and in the second row we show the

corresponding roll-angular velocity, rolling-moment coefficient and normal-force coefficient versus the roll angle. Significant transient responses develop in the time range of $t = 0 \rightarrow 22$, wherein the amplitudes of the responses increase and decrease. Thereafter, $t > 22$, the amplitudes of the responses continuously increase until $t = 95$. At $t \geq 95$, the amplitudes and frequencies of the responses become periodic reaching the limit-cycle response, which is typical of the wing-rock motion. During the limit-cycle response, the maximum roll angle, θ_{max}, is $10°$, the minimum roll angle, θ_{min}, is $-11°$ and the period of oscillation is 3.53, which corresponds to a frequency of 1.78. With $\Delta t = 0.005$, each cycle of oscillation in the limit-cycle response requires 706 time steps. The shown responses, up to $t = 140$, required 28,000 time steps. It should be noticed that the frequency of the normal-force coefficient is twice that of the roll angle and rolling-moment coefficient.

Next, we consider one cycle of the limit-cycle response and analyze the roll angle, rolling-moment-coefficient and normal-force-coefficient responses to gain physical insight of the wing-rock phenomenon. For this purpose, we show in Fig. 3 θ, M_x and C_N vz. t in the range of $t = 135.19 \rightarrow 138.72$ and the corresponding $\dot{\theta}$, M_x and C_N vz. θ in the range of $\theta = -0° \rightarrow +0°$. This period of oscillation is marked by the numbers 1, 2, 3, 4 and 5 in Fig. 3. In the first quarter of the cycle (1 $\rightarrow$ 2), the roll angle of the left side of the wing decreases from $0°$ $\rightarrow$ $-11°$ and the wing rolls in the clockwise (CW) direction, the rolling-moment coefficient increases and changes sign from $-0.057 \rightarrow 0.0 \rightarrow +0.023$ and the normal-force coefficient decreases and then increases from $2.68 \rightarrow 2.65 \rightarrow 2.75$. It is important to notice that the rolling moment changes its sign which means that the rolling moment during the first part of this quarter of the cycle is in the CW direction (the same direction as the motion) and in the second part of this quarter of the cycle is in the CCW direction (the opposite direction of the motion). Hence, the rolling moment increases the negative angle in the first part and then it limits the growth of the roll angle in the second part. In the second quarter of the cycle (2 $\rightarrow$ 3) the roll angle increases from $-11° \rightarrow 0$ and the wing rolls in the CCW direction, the rolling-moment coefficient increases and then decreases from $+0.023 \rightarrow 0.045 \rightarrow 0.04$ and the normal-force coefficients increases and then decreases from $2.75 \rightarrow 3.0 \rightarrow 2.84$. The rolling-moment coefficient is in the CCW direction (the same direction as the motion). In the third quarter of the cycle (3$\rightarrow$4) the roll angle increases from $0 \rightarrow 10°$ and the wing keeps its rolling motion in the CCW direction, the rolling-moment coefficient decreases and changes sign from $+0.04 \rightarrow 0$ $\rightarrow -0.038$ and the normal-force coefficient decreases and then increases from $2.84 \rightarrow 2.78 \rightarrow 2.86$. Again, it is noticed that the rolling moment changes its sign from CCW to CW directions and limits the roll angle growth.

In Figs. 4 and 5, we show snapshots at points 2 and 4, respectively; of the cross-flow-velocity vectors and the static-pressure contours at the chord stations of 0.54, 0.63 and 0.79 and the surface-pressure coefficient at the chord stations of 0.54 and 0.63. In Fig. 4, the primary vortex on the right side is nearer to the upper wing surface than the one on the left side. Moreover, the primary vortex on the right is further away from the plane of geometric symmetry in comparison to the one on the left. The surface-pressure curves show large peaks on the right side and that the surface-pressure difference on the right side is larger than the one on the left side. This results into a CCW rolling moment at this maximum negative roll angle of $-11°$. In Fig. 5, the opposite process occurs; the surface-pressure difference on the left side is larger than the one on the right side and this results into a CW rolling moment at this maximum positive roll angle of $+10°$. These results are consistent with those of the experimental data of Refs. 3 and 4.

In Fig. 6, we show the variations of the maximum static pressure of the vortex cores of the primary vortices on the left and right sides versus the roll angle for the chord station of 0.54. The numbers on the figures correspond to those in Fig. 3. Since the maximum static pressure of the core is proportional to the vortex-core strength, it is obviously seen that the primary vortex on the right side has a greater strength at point 2 as compared to that on the left side. The strength differential between the right and left vortices along with the locations of the vortex cores contributes substantially to the net total CCW rolling moment which limits the negative growth of the roll angle and reverses the wing motion. Similarly, it is concluded that the strength differential between the left and right vortices at point 4 substantially contributes to the net total CW rolling moment which limits the positive growth of the roll angle and reverses the wing motion.

In Fig. 7, we split the rolling-moment coefficient into restoring and damping components similar to Konstadinopoulos, et al.[9]. First, the rolling-moment coefficient M_x is fitted using the following expansions in terms of θ and $\dot{\theta}$:

$$M_x = a_1\theta + a_2\dot{\theta} + a_3\theta^3 + a_4\theta^2\dot{\theta}$$
$$+ a_5\dot{\theta}^2\theta + a_6\dot{\theta}^3 + a_7\theta^5 + a_8\theta^4\dot{\theta}$$
$$+ a_9\theta^2\dot{\theta}^3 + a_{10}\dot{\theta}^2\theta^3 + a_{11}\dot{\theta}^4\theta + a_{12}\dot{\theta}^5 \quad (13)$$

The coefficients $a_1 - a_{12}$ are determined using a least-squares fit. A comparison of the original ($-\circ-$) and fitted ($-\times-$) rolling-moment coefficients is shown in Fig. 7. Next, we split the fitted-rolling-moment coefficient into a restoring part, M_r, and a damping part, M_d, as follows:

$$M_r = \left(a_1 + a_3\theta^2 + a_{11}\dot{\theta}^4\right)\theta$$
$$+ \left(a_3 + a_{10}\dot{\theta}^2\right)\theta^3 + a_7\theta^5 \quad (14)$$

$$M_d = \left(a_2 + a_4\theta^2 + a_8\theta^4\right)\dot{\theta}$$
$$+ \left(a_6 + a_9\theta^2\right)\dot{\theta}^3 + a_{12}\dot{\theta}^5 \quad (15)$$

4

In Fig. 7, we also show M_r and θ versus time, and M_d and θ versus time. Moreover, we show on these figures the numbers 1, 2, 3, 4 and 5 which correspond to the same numbers in Figs. 3 and 6. In the first quarter of the cycle (1→2), the roll angle θ decreases from 0 → -11°, the restoring rolling moment becomes negative during the first part and positive during the second part and the damping rolling moment, which is negative at point 1, increases during the first part and becomes almost zero during the second part. It is very interesting to notice that M_r and M_d are negative during the first part and hence they are in the same direction as the motion. During the second part, M_r becomes positive reaching its maximum at point 2 when $\theta_{max} = -11°$ and hence it limits the angle growth. During the same second part, M_d becomes almost zero indicating a loss of damping rolling moment. In the second quarter of the cycle (2→3), M_r stays almost constant during the first part and drops to zero in the second part when the roll angle becomes 0°. During the same second quarter, M_d continuously increases from 0 to a maximum positive value when the roll angle becomes 0. In the third quarter of the cycle (3-4), a similar interaction of θ, M_r and M_d as that of the first quarter (1-2) occurs except with opposite signs. These conclusions are exactly similar to those of Ref. 9. Hence, the loss of damping rolling moment is responsible for the wing-rock motion.

Simulation of Wing Roll Divergence

In Ref. 10, it has been reported that roll divergence has been observed for the 80° leading-edge sweep delta wing. In fact, roll divergence has been analytically shown[10] to exist for certain initial conditions using the phase plane analysis. In the present paper, we considered the same wing described earlier to simulate roll divergence. The aerodynamic conditions are kept the same as those for the wing-rock problem. For the dynamic conditions, we set $\lambda = 0$ and $k = 0$; i.e., there is neither bearings damping nor torsional springs. The mass-moment of inertia is kept at $I_{xx} = 0.285$. Starting with the same steady flow solution of the previous problem, as the initial conditions, we released the wing at $t = 0$.

In Figs. 8-12, we show the results of this case. Figure 8 shows the roll angle, rolling-moment coefficient and normal-force coefficient versus time. The roll angle increases slowly to 10° at $t = 4.5$ (point 1) while the rolling-moment coefficient increases at a little larger rate until $t = 4.5$. The rolling-moment coefficient is in the CCW direction, which is the same direction as the motion. The normal-force coefficient increases and then decreases to almost its original value. Figure 9 shows the corresponding snapshots at point 1 of the crossflow-velocity vectors and static-pressure contours at the chord stations of 0.54 and 0.79 and the surface-pressure coefficient at the chord station of 0.79. The primary vortex on the right side is larger than the one on the left and it is nearer to the plane of geometric symmetry than the one

on the left. The surface-pressure-coefficient curve shows that a net CCW rolling-moment exists.

In the time range $t = 4.5 \to 6$ (points 1 → 2), Fig. 8 shows that the roll angle increases at a faster rate than before ($\theta = 35°$ at point 2), the rolling-moment coefficient increases at a very fast rate and the normal-force coefficient drops. Figure 10 shows the corresponding snapshots of results at point 2. The primary vortex on the right becomes larger than the one on the left. Moreover, the primary vortex on the right expands in the spanwise direction, while the one on the left moves outboard of the left leading edge. The surface-pressure-coefficient shows that the pressure coefficient on the left upper surface becomes positive. This explains the fast increase in the rolling-moment coefficient and the fast decrease in the normal force coefficient.

In the time range $t = 6 \to 6.75$ (points 2→3), Fig. 8 shows that the roll angle increases at an even faster rate than before ($\theta = 64°$ at point 3), the rolling-moment coefficient increases to a peak value and then decreases and the normal-force coefficient keeps on decreasing. Figure 11 shows the corresponding snapshots of results at point 3. The primary vortex on the right side becomes very large and affects a portion of the left side of the wing. The primary vortex on the left is already off the left leading edge. In fact, one can see the left vortex on the left lower surface of the wing. The surface-pressure curves clearly explain the loss of normal force and the increase and decrease in the rolling-moment coefficient.

In the time range of $t = 6.75 - 8.25$ (points 3→4), Fig. 8 shows that the roll angle becomes substantially high ($\theta = 138°$ at point 4), the rolling-moment coefficient decreases fast and the normal-force coefficient increases fast. Figure 12 shows the corresponding snapshots of the results at point 4. The primary vortices on the upper surface disappear and start appearing on the lower surface. The surface pressure curve shows that the pressure coefficient on the lower surface is completely negative and on the upper surface is partially positive and partially negative. The surface pressure curve explains the sudden drop in the rolling-moment coefficient and the sudden increase in the normal-force coefficients.

Concluding Remarks

Computational simulation of unsteady, three-dimensional, subsonic flows around a delta wing undergoing wing-rock and roll-divergence motions is presented and analyzed. The present multidisciplinary problem is solved for the first time using sequential solutions of the three-dimensional unsteady Euler equations for the flowfield and the Euler equation of rigid-body rolling motion for the wing kinematics. The fluid flow Euler equations are solved using an implicit, approximately factored, central-difference, finite-volume scheme and the rigid-body Euler equation is solved using a four-stage, Runge-Kutta scheme. Simulation of the wing-rock problem is obtained

for a delta wing which is mounted on an axle with torsional springs and the axle is free to rotate in bearings with viscous damping. The wing starts its motion under the effect of an initial rolling moment due to the initially asymmetric flow at zero roll angle and zero angular velocity. For the simulation of the roll-divergence problem, the bearings are assumed frictionless and the torsional springs are removed. It has been shown that the hysteresis responses of position and strength of the asymmetric right and left primary vortices are responsible for the wing rock motion. Moreover, it has also been shown that the loss of aerodynamic damping rolling moment at the zero angular velocity value is a main reason for the wing rock motion. These conclusions are consistent with the previous findings of the experimental[3,4] and computational[9] research work.

Acknowledgement

References

1. Nguyen, L. T., Yip, L. and Chambers, X., Jr., "Self-Induced Wing Rock of Slender Delta Wings," AIAA Paper No. 81-1883, August 1981.

2. Levin, D. and Katz, J., "Dynamic Load Measurements with Delta Wings Undergoing Self-Induced Roll-Oscillations," Journal of Aircraft, Vol. 21, January 1985, pp. 30-36.

3. Jun, Y. W. and Nelson, R. C., "Leading Edge Vortex Dynamics on a Delta Wing Undergoing a Wing Rock Motion," AIAA-87-0332, January 1987.

4. Arena, A. S., Jr. and Nelson, R. C., "The Effect of Asymmetric Vortex Wake Characteristics on a Slender Delta Wing Undergoing Wing Rock Motion," AIAA 89-3348-CP, August 1989, pp. 16-24.

5. Morris, S. L. and Ward, D. T., "A Video-Based Experimental Investigation of Wing Rock," AIAA 89-3349-CP, August 1989, pp. 25-35.

6. Arena, A. S. and Nelson, R. C., " Unsteady Surface Pressure Measurements on a Slender Delta Wing Undergoing Limit Cycle Wing Rock," AIAA paper No. 91-0434, January 1991.

7. Ericsson, L. E., "The Fluid Mechanics of Slender Wing Rock," Journal of Aircraft, Vol. 21, May 1984, pp. 322-328.

8. Ericsson, L. E., "Various Sources of Wing Rock," Journal of Aircraft, Vol. 27, June 1990, pp. 488-494.

9. Konstandinopoulos, P., Mook, D. T. and Nayfeh, A. H., "Subsonic Wing Rock of Slender Delta Wings,"

Journal of Aircraft, Vol. 22, March 1985, pp. 223-228.

10. Elzebda, J. M., Nayfeh, A. H. and Mook, D. T., "Development of an Analytical Model of Wing Rock for Slender Delta Wings," Journal of Aircraft, Vol. 26, August 1989, pp. 737-743.

11. Nayfeh, A. H., Elzebda, J. M. and Mook, D. T., "Analytical Study of the Subsonic Wing-Rock Phenomenon for Slender Delta Wings," Journal of Aircraft, Vol. 26, September 1989, pp. 805-809.

12. Hsu, C. and Lan, C. E., "Theory of Wing Rock," Journal of Aircraft, Vol. 22, Oct. 1985, pp. 920-924.

13. Kandil, O. A. and Chuang, H. A., "Computation of Steady and Unsteady Vortex Dominated Flows with Shock Waves," AIAA Journal, Vol. 26, No. 5, 1988, pp. 524-531.

14. Kandil, O. A. and Chuang, H. A., "Unsteady Transonic Airfoil Computation Using Implicit Euler Scheme on Body-Fixed Grid," AIAA Journal, Vol. 27, No. 8, August 1989, pp 1031-1037.

15. Kandil, O. A. and Chuang, H. A., "Unsteady Delta-Wing Flow Computation Using an Implicit Factored Euler Scheme," First National Fluid Dynamics Congress, July 1988. Also AIAA Journal, Vol. 28, No. 9, September 1990, pp. 1589-1595.

16. Kandil, O. A. and Chuang, H. A., "Unsteady Navier-Stokes Computations Past Oscillating Delta Wing at High Incidence," AIAA-89-0081, January 1989. Also AIAA Journal, Vol. 28, No. 9, September 1990, pp. 1565-1572.

17. Batina, J. T., "Vortex-Dominated Conical-Flow Computations Using Unstructured Adaptively-Refined Meshes," AIAA Journal, Vol. 28, No. 11, Nov. 1990, pp. 1925-1932.

18. Lee, E. M. and Batina, J. T., "Conical Methodology for Unsteady Vortical Flows about Rolling Delta Wings," AIAA-91-0730, January 1991.

19. Kandil, O. A. and Salman, A. A., "Unsteady Vortex-Dominated Flow Around Wings with Oscillating Leading-Edge Flaps," AIAA 91-0435, January 1991.

20. Kandil, O. A. and Salman, A. A., "Unsteady Supersonic Flow Around Delta Wings with Symmetric and Asymmetric Flaps Oscillation," AIAA 91-1105-CP, April 1991, Vol. 3, pp. 1888-1903.

21. Kandil, O. A. and Salman, A. A., "Effect of Leading-Edge Flap Oscillation on Unsteady Delta Wing Flow and Rock Control," AIAA-91-1796, June 1991.

22. Kandil, O. A. and Salman, A. A., "Recent Advances in Unsteady Computations and Applications of Vortex Dominated Flows," Invited paper, 4th International Symposium on Computational Fluid Dynamics, University of California, Davis, September 9-12, 1991, pp. 570-575.
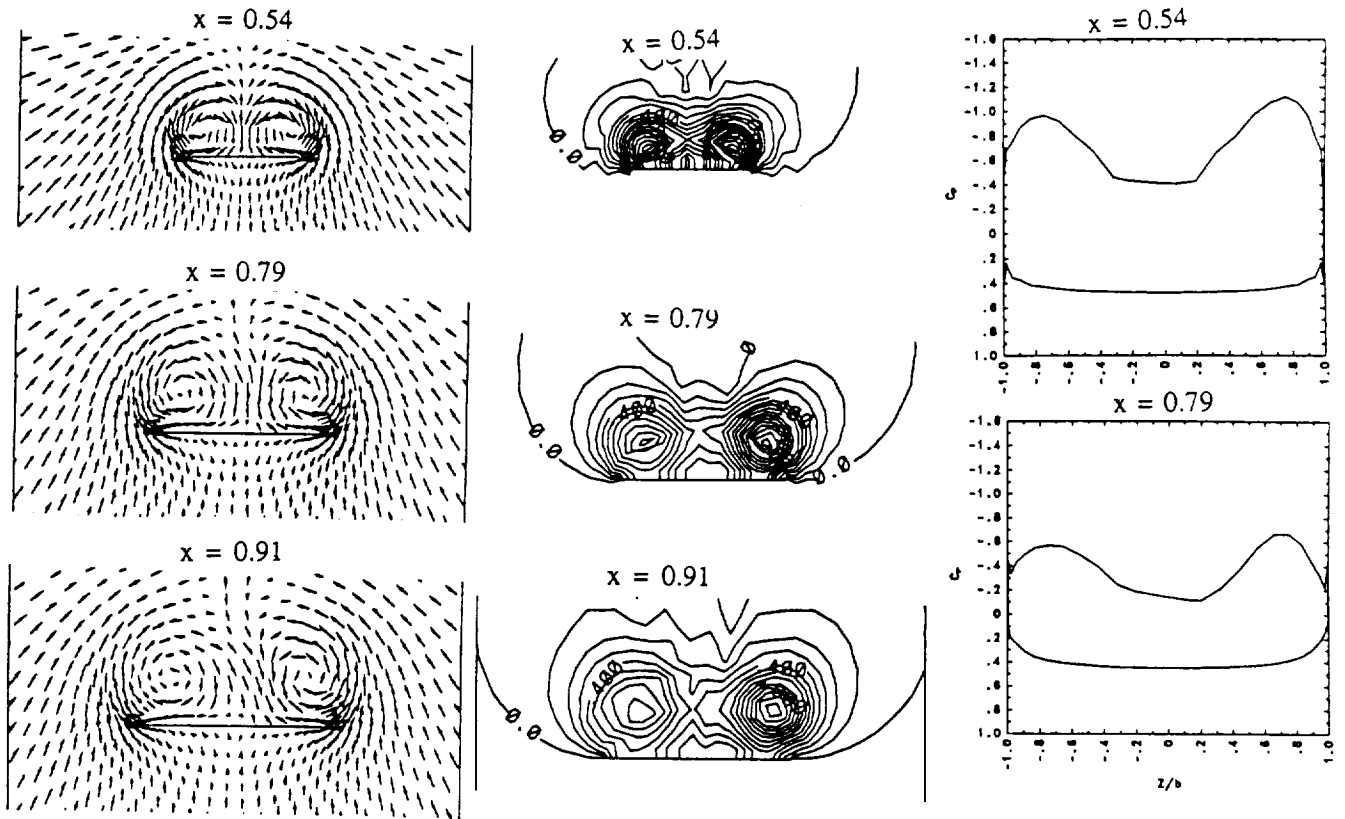
Fig. 1. Steady flow solution; crossflow velocity, static-pressure contours and surface pressure; delta wing, $\alpha = 30°$, $M_\infty = 0.3$.
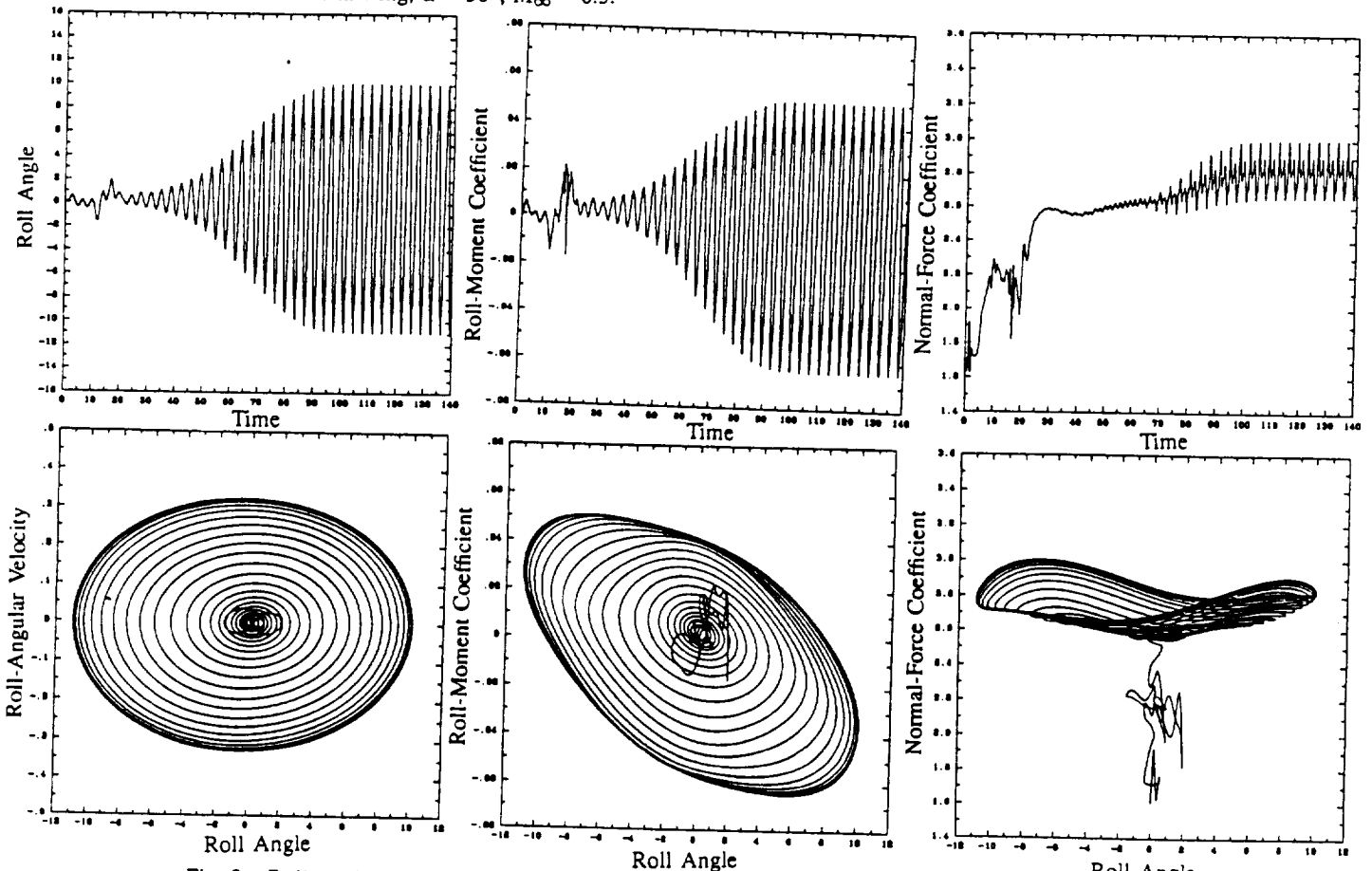

Fig. 2. Roll angle, rolling-moment-coefficient, normal-force-coefficient and phase-planes responses for wing-rock motion; delta wing, $\alpha = 30°$, $M_\infty = 0.3$, $I_{xx} = 0.285$, $\lambda = 0.15$, $\hat{k} = 0.74$, $\theta_o = \dot{\theta}_o = 0$.
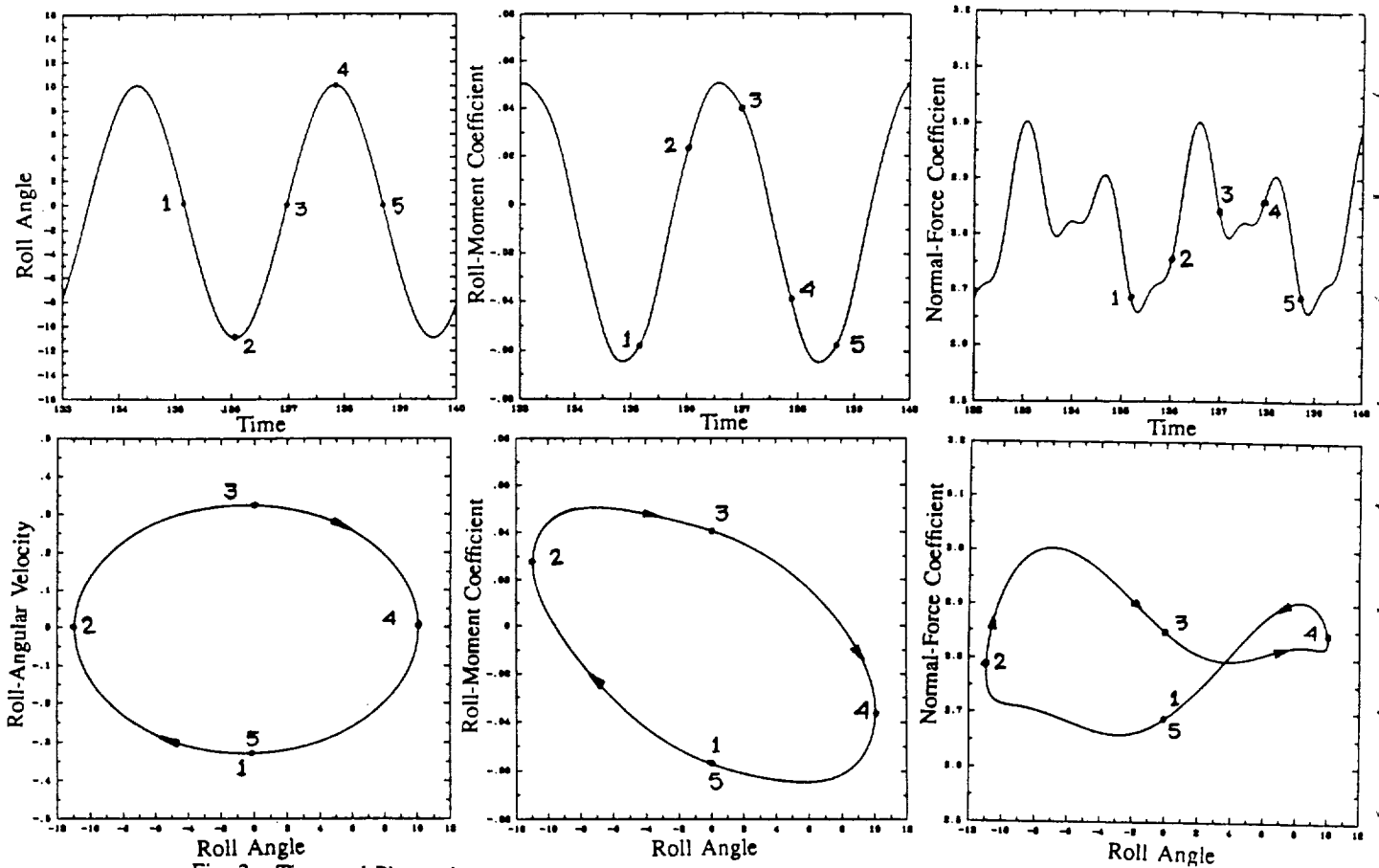
7

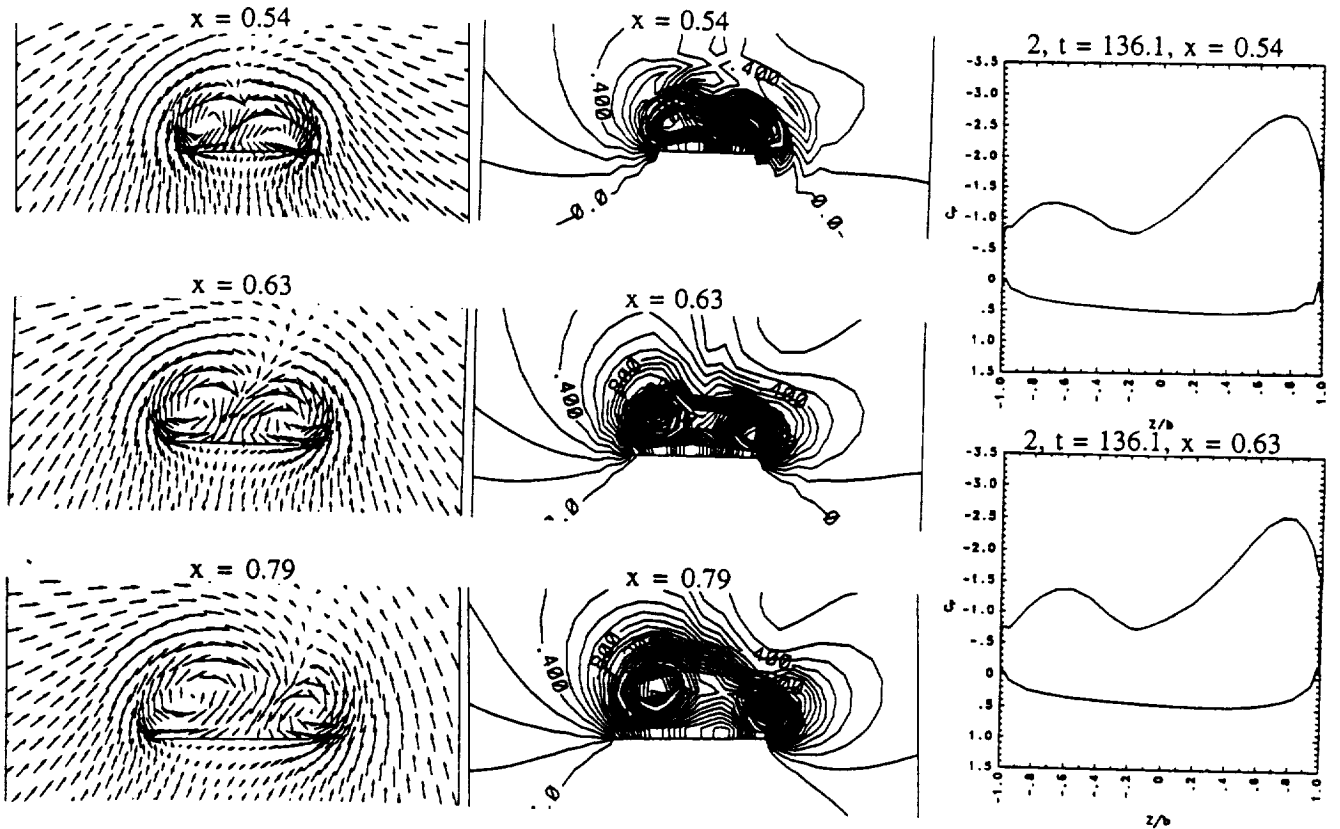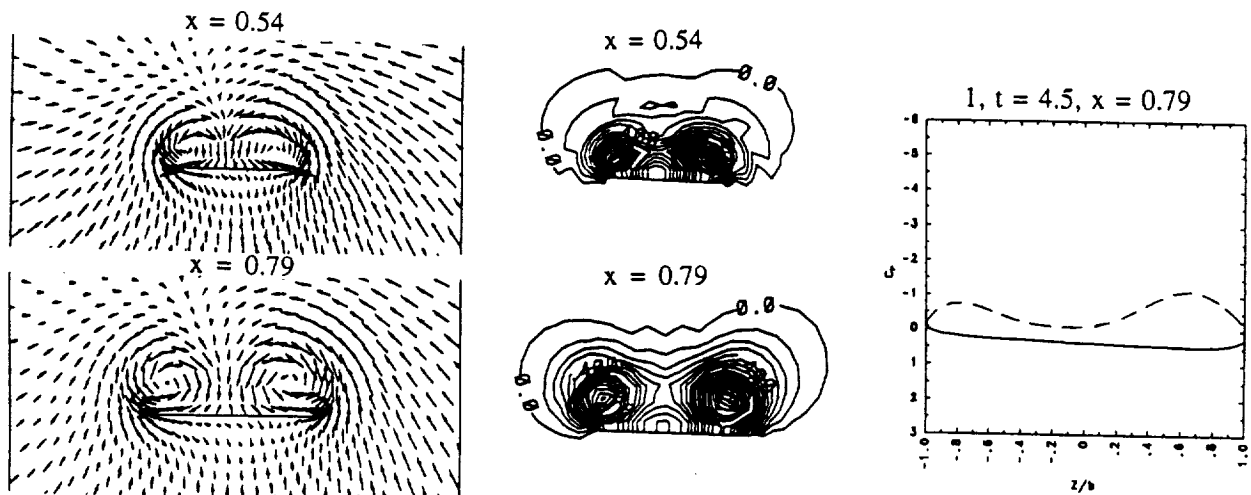Fig. 3. Time and Phase-plane responses for wing-rock motion during the limit cycle response.

Fig. 4. Snapshot at point 2 of crossflow velocity, static-pressure contours and surface pressure for wing-rock motion.

8
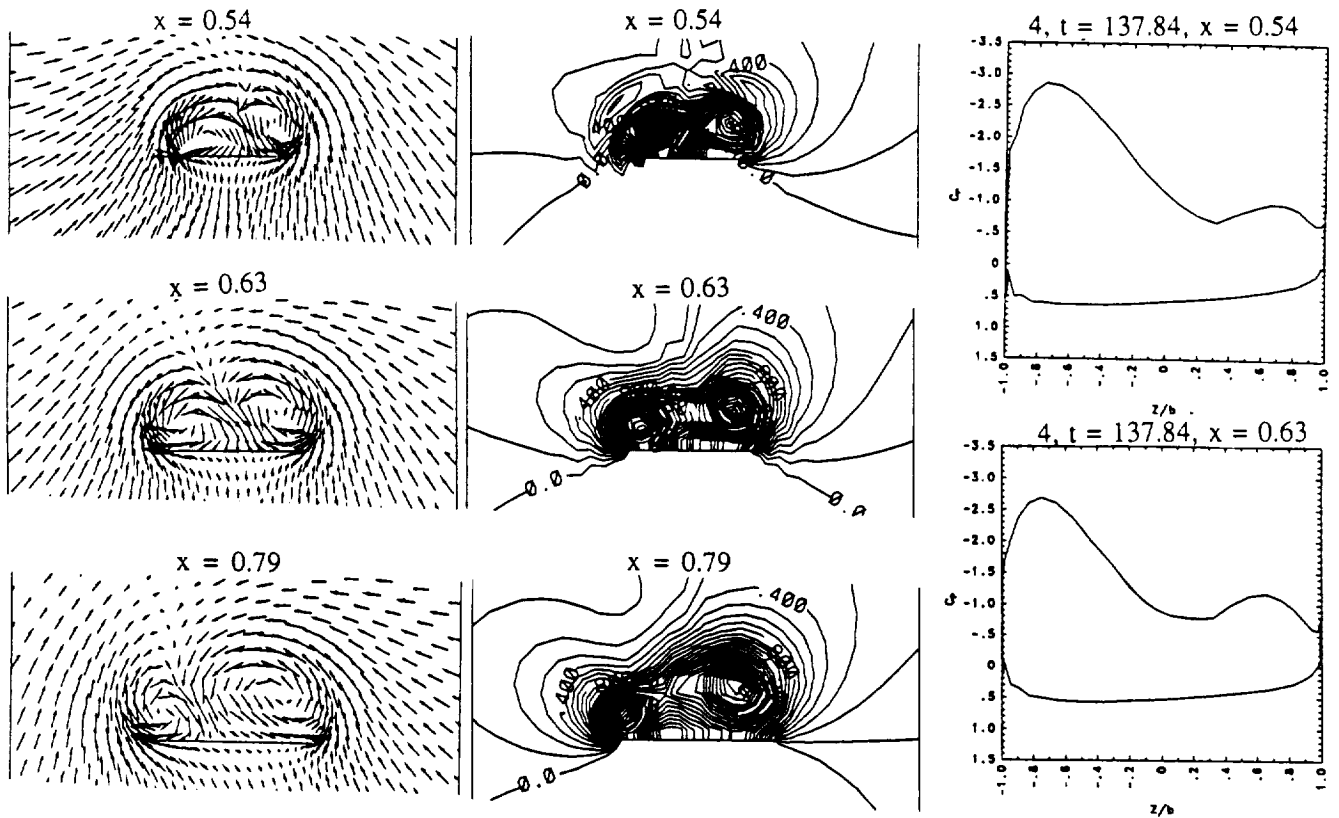
Fig. 5. Snapshot at point 4 of cross flow velocity, static-pressure contours and surface pressure for wing-rock motion.
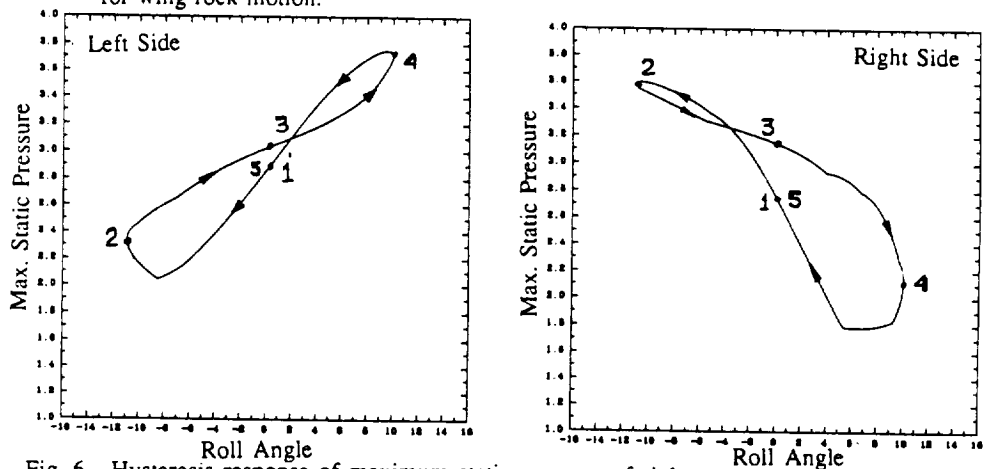
Fig. 6. Hysteresis response of maximum static pressure of right and left primary vortices for wing-rock motion during the limit-cycle response.
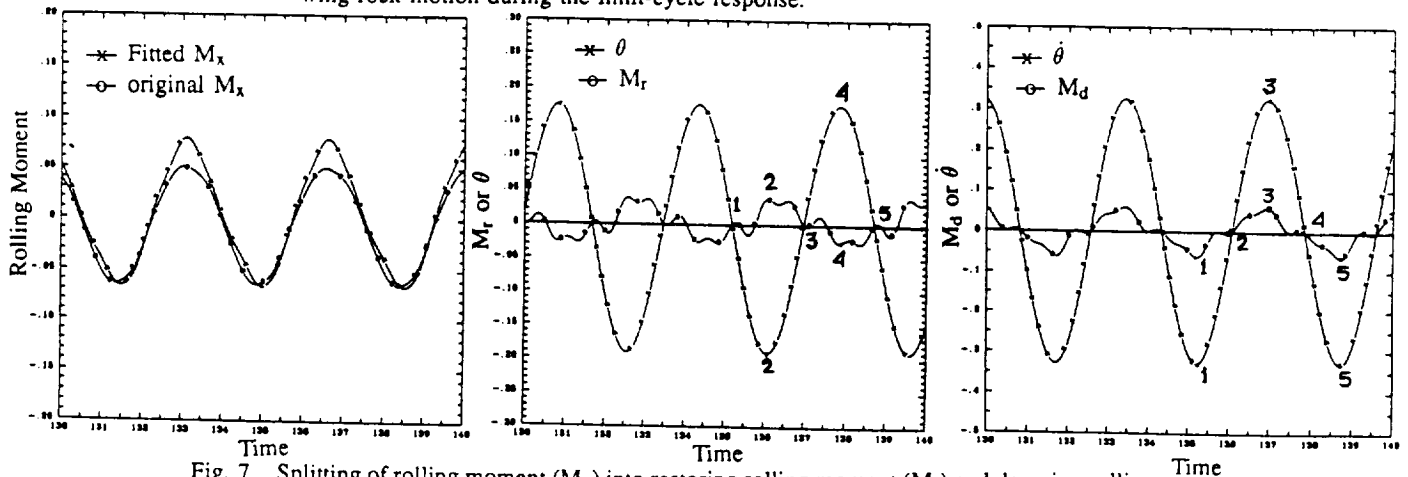
Fig. 7. Splitting of rolling moment (M_x) into restoring rolling moment (M_r) and damping rolling moment (M_d) for wing-rock motion during the limit-cycle response.

9
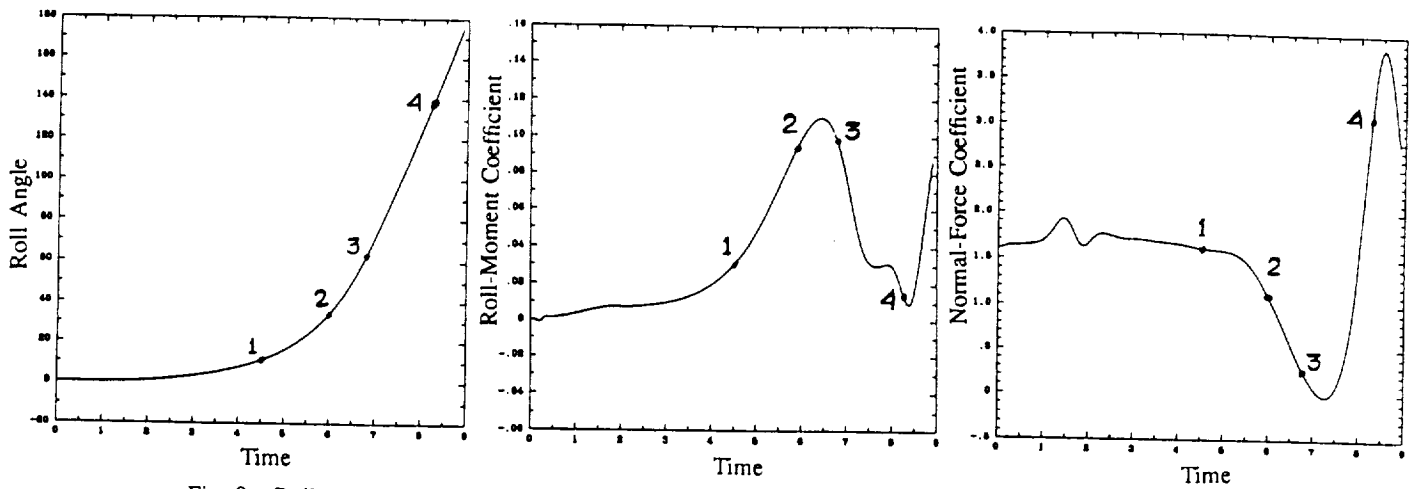
Fig. 8. Roll angle, rolling-moment-coefficient and normal-force-coefficient responses for wing roll-divergence motion; delta wing, $\alpha = 30°$, $M_\infty = 0.3$, $I_{xx} = 0.285$, $\lambda = 0$, $\hat{k} = 0$, $\theta_o = \dot{\theta}_o = 0$.

Fig. 9. Snapshot at point 1 of crossflow velocity, static-pressure contours and surface pressure for wing roll-divergence motion.
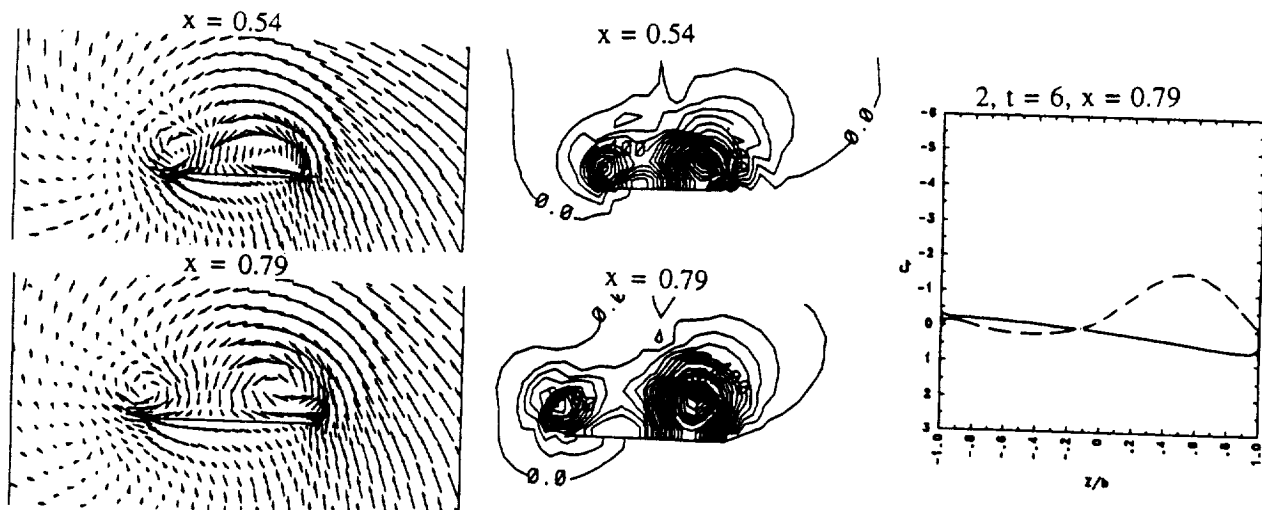
Fig. 10. Snapshot at point 2 of crossflow velocity, static-pressure contours and surface pressure for wing roll-divergence motion

10
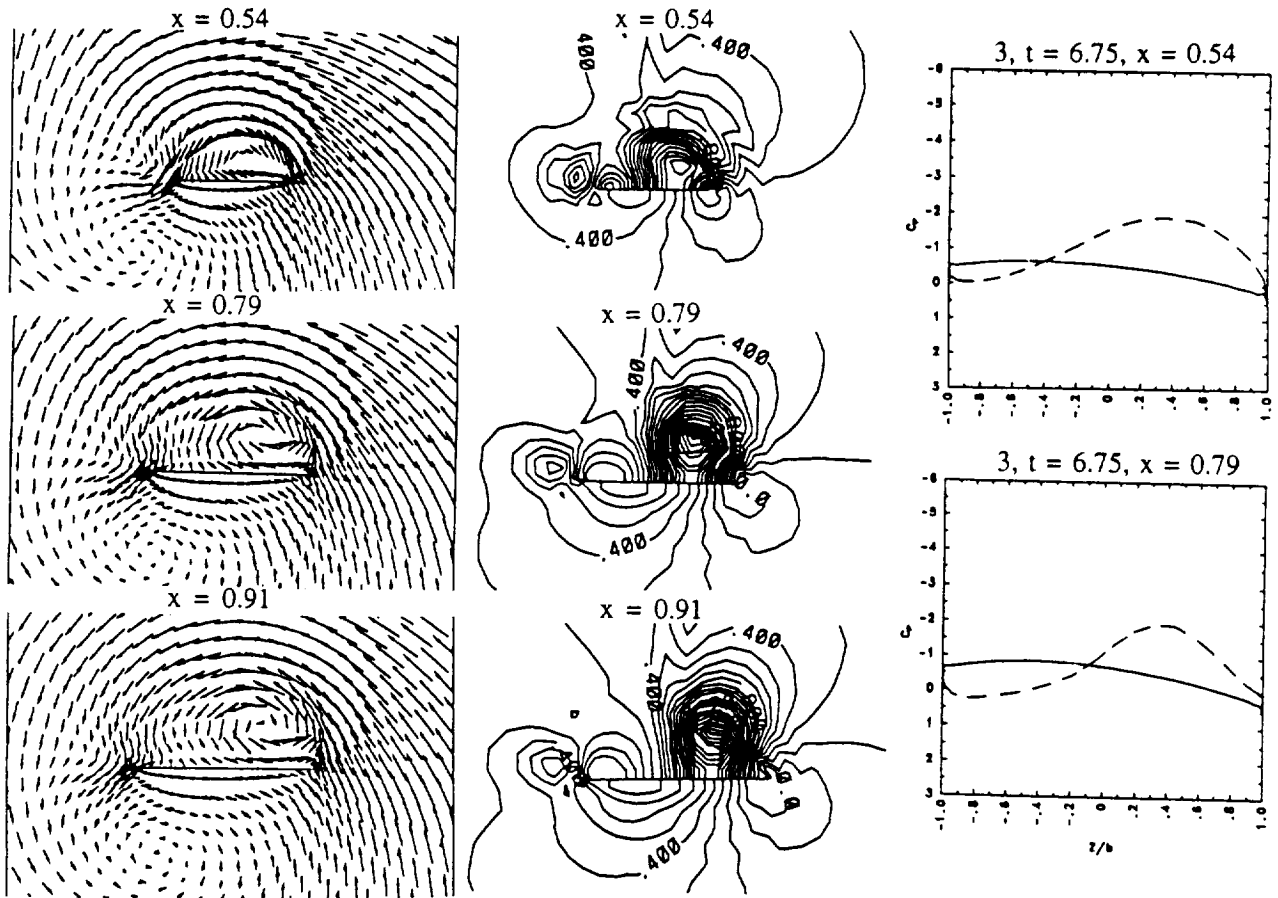
Fig. 11. Snapshot at point 3 of crossflow velocity, static-pressure contours and surface pressure for wing roll-divergence motion.

Fig. 12. Snapshot at point 4 of crossflow velocity, static-pressure contours and surface pressure for wing roll-divergence motion.

11
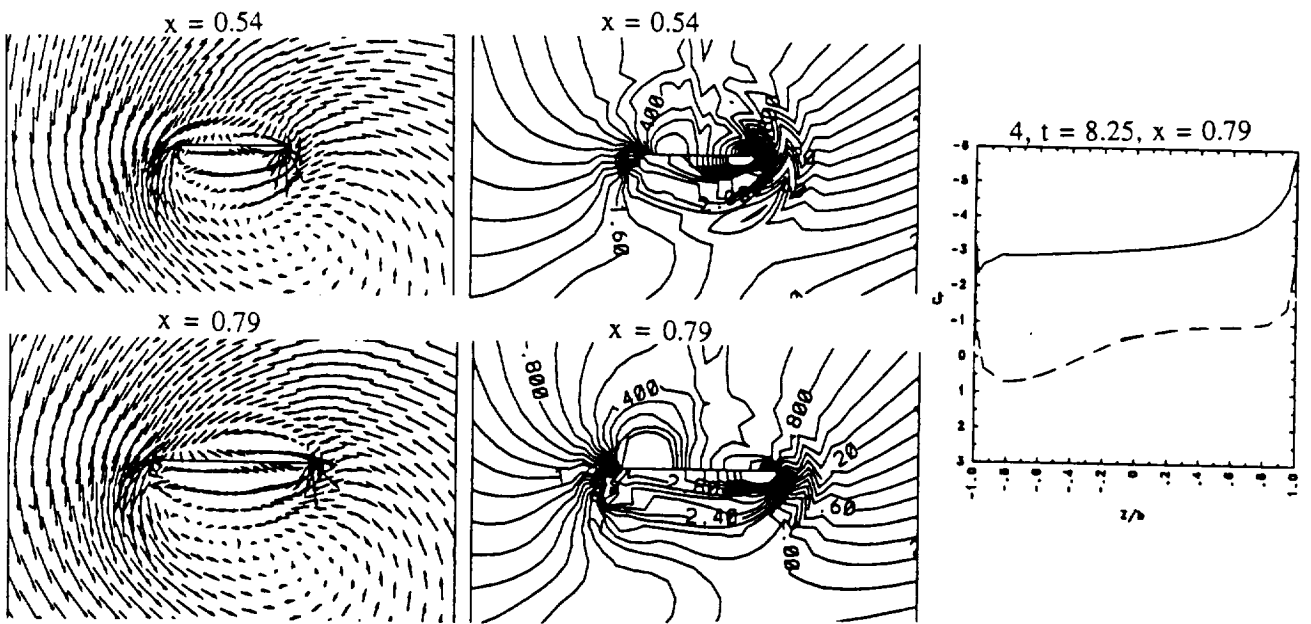
ICAS 92-4.7.2

PREDICTION AND CONTROL OF SLENDER WING ROCK

Osama A. Kandil and Ahmed A. Salman
Old Dominion University, Norfolk, Virginia, USA

18th Congress, International
Council of the Aeronautical Sciences

Beijing, Peoples Republic of China
September 20-25, 1992

PREDICTION AND CONTROL OF SLENDER-WING ROCK

Osama A. Kandil* and Ahmed A. Salman**
Old Dominion University, Norfolk, VA 23529, USA

ABSTRACT

The unsteady Euler equations and the Euler equations of rigid-body dynamics, both written in the moving frame of reference, are sequentially solved to simulate the limit-cycle rock motion of slender delta wings. The governing equations of fluid flow and dynamics of the present multi-disciplinary problem are solved using an implicit, approximately-factored, central-difference like, finite-volume scheme and a four-stage Runge-Kutta scheme, respectively. For the control of wing-rock motion, leading-edge flaps are forced to oscillate anti-symmetrically at prescribed frequency and amplitude which are tuned in order to suppress the rock motion. Since the computational grid deforms due to the leading-edge flaps motion, the grid is dynamically deformed using the Navier-displacement (ND) equations. Computational applications cover locally-conical and three-dimensional solutions for the wing-rock simulation and its control.

INTRODUCTION

The dynamic phenomenon of wing rock is characterized by large-amplitude, high-frequency, rolling oscillation with a limit-cycle amplitude. The rolling oscillation is self excited and it is triggered by vortex-flow asymmetry or vortex breakdown on highly swept delta wings at high angles of attack. The study of this phenomenon is vital for the dynamic stability and controllability of high performance aircraft during maneuvering and landing.

The literature shows that several experimental investigations[1-6] have been conducted to gain basic understanding of the phenomenon. Nguyen, et al.[1] tested a flat-plate delta wing with 80° leading-edge sweep for forced-oscillation, rotary and free-to-roll tests. The free-to-roll tests showed that the wing exhibited a rock motion at angles of attack greater than 25°, and that the rock motion reached the same limit-cycle response irrespective of the initial conditions. Levin and Katz[2] tested two delta wings with leading-edge sweeps of 76° and 80°. They found that only the wing with the 80° sweep would undergo a rock motion. Nelson and his co-workers[3-5] conducted a series of experimental studies to investigate the mechanisms responsible for wing rock on a delta wing with 80° leading-edge sweep. Their analysis revealed that the primary mechanism for the phenomenon was a time lag in the position of the vortices normal to the wing surface. Moreover, they concluded, through the analysis of separate contributions of the wing upper and lower

surface-pressure distributions, that the upper surface pressure provides all of the instability and little damping in the roll moment and that the lower surface pressure provides the classical roll damping hysteresis. Morris and Ward[6] conducted dynamic measurements in both a water tunnel and a wind tunnel on a delta wing with leading-edge sweep of 80°. Their results showed that the measured hysteresis loops in the water tunnel were opposite in direction to those of the wind tunnel. They concluded that the hysteresis direction does not play as decisive a role as previously thought in initiating and sustaining wing rock.

Erickson[7,8] analyzed experimental data for aircraft configurations at high angles of attack in an attempt to reveal the flow processes which generate wing rock. He concluded that wing rock phenomenon for slender wings is caused by asymmetric-leading-edge vortices and that the vortex breakdown provides a limiter to the growth of wing-rock amplitude. He also identified another two mechanisms for limit-cycle oscillations in roll for advanced aircraft.

The literature review showed that numerical simulation of this phenomenon for low speeds has recently been presented by Konstadinopoulos, et al.[9]. This has been followed by developments of analytical models to investigate the parameters affecting this phenomenon. Nayfeh, et al.[10-11] have presented two analytical models and Hsu and Lan[12] have presented one analytical model. The improved analytical model of Nayfeh, et al.[11] proved to be superior in comparison with the Hsu and Lan model and more accurate than their first model of reference[10]. The model of reference[11] accurately fitted the rolling moment coefficient, which was computed by a vortex-lattice method, using five terms which included the linear aerodynamic damping and restoring moments and the nonlinear aerodynamic damping moments. With this model, it was shown on the phase plane that both the wing rock and wing-roll divergence were possible responses for the wing. Hsu and Lan's model cannot predict wing-roll divergence. A serious question which can be raised regarding the work in references 9-12 is: how accurate the fluid dynamics solution is, using the vortex lattice method? Moreover, the fluid dynamics model limits its applicability to low-speed flows and to angles of attack below the critical value for vortex breakdown. Moreover, the vortex lattice model also cannot predict separated flows from smooth surfaces.

*Professor and Eminent Scholar, Department of Mechanical Engineering and Mechanics, Associate Fellow AIAA
**Graduate Student, Same Department, Member AIAA.

1

The first computational unsteady solution for the forced-rolling oscillation of a delta wing, which was based on the unsteady Euler equations, was presented by Kandil and Chuang[13]. The solution used the locally-conical flow assumption for supersonic flows in order to reduce the computational time by an order of magnitude as compared to that of the three-dimensional solutions. Forced-pitching oscillation of airfoils were also considered in a later paper by Kandil and Chuang[14]. The first unsteady three-dimensional Euler solution for the forced-pitching oscillation of a delta wing was also presented by Kandil and Chuang[15]. The unsteady Navier-Stokes solutions were also used by Kandil and Chuang[16] for the forced-rolling oscillation of a delta wing under the locally-conical flow assumption. Batina[17] developed a conical Euler solver, which was based on the use of un-structured grids, and used it to solve for the flow around a delta wing undergoing forced-rolling oscillation under the locally-conical flow assumption. Later on, Lee and Batina[18] extended the Euler solver to include a free-to-roll capability to solve for a freely rolling delta wing which exhibited wing rock. The solution was based on the locally-conical flow assumption. In Ref. 19, the present authors studied symmetric and anti-symmetric forced-rolling oscillations of the leading-edge flaps of a delta wing. A hinge is considered at the 75% location of the local half span and the leading-edge flaps are forced to oscillate both symmetrically and anti-symmetrically. The Navier-Stokes and Euler equations are used to solve the problem along with the Navier-displacement equation to account for the grid deformation due to the leading-edge flaps motion. In a later paper by the authors[20], the effects of symmetric and anti-symmetric flaps oscillation with varying frequencies have been investigated for two flow conditions. With the aid of these studies, the authors[21,22] studied the wing rock phenomenon as well as its active control using anti-symmetric tuned oscillations of the wing leading-edge flaps. The sequential solutions of unsteady Euler equations and the Navier-displacement equations along with the Euler equation of rigid-body rolling motion were used to obtain the solutions for these problems. The locally-conical flow assumption was also used throughout these solutions. Simulation of wing-rock and wing-divergence motions was presented by the authors for the three-dimensional flows in Ref. 23.

In the present paper, the unsteady Euler equations and the Euler equations of rigid-body dynamics, both written in the moving frame of reference, are used to simulate the limit-cycle rock motion of slender delta wings. Controlling the wing-rock motion is achieved by using anti-symmetric forced-oscillation of the wing leading-edge flaps. For the active control of wing rock, the grid is dynamically deformed using the ND equations.

FORMULATION

The formulation of the problem consists of three sets of equations. The first set is the unsteady, compressible, Euler equations which are written relative to a moving frame of reference. This set is used to compute the flowfield for steady or unsteady flows. The second set is the unsteady, linearized, Navier-displacement equations which are used in the moving frame of reference to compute the grid displacements whenever the leading-edge flaps oscillate. If the leading-edge flaps do not oscillate, the ND equations are not used. The third set is the Euler equations of rigid-body motion for the wing only or for the wing and its flaps. This set is used to compute the wing motion for the wing-rock problem. It is solved in sequence with the first set. For the control of wing-rock motion, this set is solved in sequence with the first and second sets.

Unsteady Euler Equations

Using the transformation equations from the space-fixed frame of reference to a moving frame of reference (Refs. 13-15), the non-dimensional, unsteady, compressible, Euler equations are transformed to the moving frame of reference. Such a transformation eliminates the motion of the computational grid for rigid wings having time-dependent rigid-body motion. Since the flaps of the wings are allowed very small relative rigid-body motion per time step of the integration scheme, one must consider the computational grid as time-dependent whenever the grid is updated, and the grid speed in Eqs. (4) and (5) must be computed. Hence, the Euler equations are given by

$$\frac{\partial \bar{Q}}{\partial t} + \frac{\partial \bar{E}_l}{\partial \xi^l} = \bar{S} \qquad (1)$$

where

$\bar{Q} \equiv$ flowfield vector

$$= \frac{\hat{q}}{J} = \frac{1}{J}[\rho, \rho u_1, \rho u_2, \rho u_3, \rho e]^t \qquad (2)$$

$$\xi^m = \xi^m(x_1, x_2, x_3, t) \qquad (3)$$

$\bar{E}_m \equiv$ inviscid flux

$$= \frac{1}{J}\left(\partial_k \xi^m \hat{E}_k + \frac{\partial \xi^m}{\partial t}\hat{q}\right)$$

$$= \frac{1}{J}[\rho U_m, \rho u_1 U_m + \partial_1 \xi^m p, \rho u_2 U_m$$

$$+ \partial_2 \xi^m p, \rho u_3 U_m + \partial_3 \xi^m p, \rho U_m h - \frac{\partial \xi^m}{\partial t}p]^t \qquad (4)$$

$$U_m = \partial_k \xi^m u_k + \frac{\partial \xi^m}{\partial t} \qquad (5)$$

2

$\bar{S} \equiv$ source term due to rigid–body motion $= \dfrac{1}{J}\hat{S}$

$= \dfrac{1}{J}\{0, -p(a_t)_1, -p(a_t)_2, -p(a_t)_3, -p[\bar{V} \cdot \bar{a}_o$
$+ (\bar{\omega}x\bar{r}) \cdot \bar{a}_o + \bar{V}_o \cdot (\bar{a}_t - \bar{\omega}x\bar{V}) + \bar{V} \cdot (\dot{\bar{\omega}}x\bar{r})$
$+ (\bar{\omega}x\bar{r}) \cdot (\bar{\omega}x\bar{r})]\}^t$ (6)

$$\bar{V} = \bar{V}_a - \bar{V}_t \equiv \text{ relative velocity} \qquad (7)$$

$$\bar{V}_t = \bar{V}_o + \bar{\omega}x\bar{r} \qquad (8)$$

$$\bar{a}_t = \bar{a}_o + \dot{\bar{\omega}}x\bar{r} + 2\bar{\omega}x\bar{V}_o + \bar{\omega}x(\bar{\omega}x\bar{r}) \qquad (9)$$

$$p = \rho(\gamma - 1)\left(e - \frac{V^2}{2} + \frac{V_t^2}{2}\right) \qquad (10)$$

$$h = \frac{\gamma p}{\rho(\gamma - 1)} + \frac{V^2}{2} - \frac{V_t^2}{2} \qquad (11)$$

The reference parameters for the dimensionless form of the equations are $L, a_{\infty}, L/a_{\infty}$ and ρ_{∞} for the length, velocity, time and density, respectively. Here, L is a reference length which is taken as the wing root-chord length.

In Eqs. (1)-(11), the indicial notation is used for convenience. Hence the indices k, l, n and s are summation indices and m is a free index. The range of $k, l, m, n,$ and s is 1–3 and $\partial_k \equiv \frac{\partial}{\partial x_k}$.

The term $\frac{\partial \xi^m}{\partial t}$ represents the mth component of the grid velocity. It is set equal to zero when the grid is not being updated. In Eqs. (1)-(11), ρ is the density, u_n the relative fluid velocity component, $\bar{V}_o$ and $\bar{a}_o$ translation velocity and acceleration of the moving frame, $\bar{V}_t$ and $\bar{a}_t$ the transformation velocity and acceleration from the space-fixed to the moving frames of reference, $\bar{\omega}$ and $\dot{\bar{\omega}}$ the angular velocity and acceleration of the moving frame, $\bar{r}$ the fluid position vector, p the pressure, e and h the total energy and enthalpy per unit mass relative to the moving frame and γ the gas index which is set equal to 1.4.

Unsteady, Linearized Navier-Displacement Equations

The details of the derivation of these equations are given by the authors in Ref. 20. The dimensionless form of these equations is given by

$$-\nabla p + \frac{\mu M_{\infty}}{R_{em}} \frac{\partial}{\partial t}\left[\frac{1}{3}\nabla(\nabla \cdot \bar{u}) + \nabla^2\bar{u}\right] = \rho\frac{\partial^2\bar{u}}{\partial t^2} \quad (12)$$

where $\bar{u}$ is the displacement vector of a grid point. For each grid point (a fluid element), Eq. (12) is integrated

over a short time range $(t - t_o)$ where λ, μ and ρ are kept constants. This yields the equation

$$-\int_{t_o}^{t} \nabla p dt + \frac{\mu M_{\infty}}{R_{em}}\left[\frac{1}{3}\nabla(\nabla \cdot \bar{u}) + \nabla^2\bar{u}\right]$$
$$= \rho\frac{\partial\bar{u}}{\partial t} + \hat{C}_o(\bar{r}) \qquad (13)$$

In Eq. (12), we use R_{em} to refer to the mesh point Reynolds number which is different from the flow Reynolds number. This has been done in order to provide a limiter for the grid displacement to avoid grid distortion or overlapping, particularly in regions of high flow reversal. Equation (13) is the vector form of the ND equations to be used for computing the grid-points displacement $\bar{u}$ subject to displacement boundary and initial conditions. The equation is a parabolic equation in time which is integrated by using the alternating direction implicit (ADI) scheme. The constant $\hat{C}_o(\bar{r})$ in Eq. (13) is computed from the preceding time-range integrations.

Euler Equation of Rolling Rigid Wing With and Without Oscillating Leading-Edge Flaps:

Figure 1 shows a sketch of a wing and its flaps which are undergoing rolling motions. The rolling motion of the flaps is anti-symmetric. The wing is fixed to an axle which rotates in bearings. The bearings damping coefficient is λ. Torsional springs of stiffness $\hat{k}$ are assumed at the ends of the axle. The xyz axes which are fixed to the wing are assumed to coincide with the principal axes of inertia of the wing-flaps configuration. At section A-A, the wing half span is l_1 and the flap width is l_2. The masses of the wing and each flap are m_1 and m_2, respectively, and their respective mass-moment of inertias around their centers of mass are I_{c1} and I_{c2}. The generalized coordinates of the system are taken as θ_1 and θ_2, which are measured from the horizontal position. If the aerodynamic moment of the wing and its flaps about the x-axis is C_r and if one uses the Lagrangian dynamics for obtaining the governing equations of motion, one gets the following equation for the θ_1 coordinate

$$C_r - \left(2I_{ss2} - \frac{m_2}{2}l_2^2 - m_2l_1l_2\cos\theta_{21}\right)\ddot{\theta}_{21}$$
$$+ m_2l_1l_2\dot{\theta}_{21}^2\sin\theta_{21}$$
$$= \left(I_{ss1} + 2I_{ss2} - \frac{m_2}{2}l_2^2 - m_2l_1l_2\cos\theta_{21}\right)\ddot{\theta}_1$$
$$- m_2l_1l_2\dot{\theta}_1^2\sin\theta_{21}$$
$$- 2m_2l_1l_2\dot{\theta}_1\dot{\theta}_{21}\sin\theta_{21} + \lambda\dot{\theta}_1 + \hat{k}\theta_1 \qquad (14)$$

where $\theta_{21} = \theta_2 - \theta_1$, I_{1ss} and I_{2ss} are the mass moment of inertia of the wing and the flap, respectively, around the wing axis of rotation. If the angles θ_1 and θ_{21} are assumed to be small, then the linearized equation reduces to

$$C_r - \left(2I_{ss2} - \frac{m_2}{2}l_2^2 - m_2l_1l_2\right)\ddot{\theta}_{21}$$
$$= \left(I_{ss1} + 2I_{ss2} - \frac{m_2}{2}l_2^2 - m_2l_1l_2\right)\ddot{\theta}_1$$
$$+ \lambda_1\dot{\theta}_1 + \hat{k}\theta_1 \qquad (15)$$

3

On the other hand, if the flaps are not deflected and the wing and its flaps roll as a rigid body, Eq. (15) becomes

$$C_r = I_{xx}\ddot{\theta}_1 + \lambda\dot{\theta}_1 + \hat{k}\theta_1 \qquad (16)$$

where I_{xx} is the mass moment of inertial of the composite wing-flaps configuration without relative motion.

Equation (16) governs the wing-rock problem while Eq. (15) governs the linearized control of wing-rock problem by using a prescribed motion of the leading-edge flaps.

COMPUTATIONAL SCHEMES

The computational scheme used to solve Eqs. (1)-(11) is an implicit, approximately-factored, centrally-differenced, finite-volume scheme[13-15]. Added second-order and fourth-order explicit dissipation terms are used in the difference equation on its right-hand side terms, which represent the explicit part of the scheme. The Jacobian matrices of the implicit operator on the left-hand side of the difference equation are centrally-differenced in space, and implicit second-order dissipation terms are added for the scheme stability. The left-hand side spatial operator is approximately factored and the difference equation is solved in three sweeps in the ξ^1, ξ^2 and ξ^3 directions, respectively.

For the wing-rock problem, Eq. (16) is solved using a four-stage Runge-Kutta scheme. Starting from known initial conditions for θ and $\dot{\theta}$, the equation is explicitly integrated in time in sequence with the fluid dynamics equations, Eqs. (1-11). Equation (16) is used to solve for θ, $\dot{\theta}$ and $\ddot{\theta}$ while Eqs. (1-11) are used to solve for C_r. If the initial C_r is nonzero, a case of asymmetric steady flow at initial conditions, the initial values of θ and $\dot{\theta}$ are set equal to zero and the motion is initiated by the initial rolling moment.

For the control of the wing-rock problem using flaps oscillation, the motion of the flaps; θ_{21}, $\dot{\theta}_{21}$ and $\ddot{\theta}_{21}$ are specified and Eq. (14) (nonlinear equation) or Eq. (15) (linearized equation) is used to solve for θ_1, $\dot{\theta}_1$ and $\ddot{\theta}_1$. The fluid dynamics equations, Eqs. (1)-(11), and the grid-deformation equation, Eq. (13), are sequentially used to solve for C_r.

COMPUTATIONAL APPLICATIONS AND DISCUSSION

Simulation of Wing-Rock-Motion (Locally-Conical Flow)

A delta wing of sweep-back angle of 80°, at an angle of attack of 35° and a Mach number of 1.4 is considered. The wing has an elliptic section with sharpened leading edges. The wing mass-moment of inertia about its x axis is 0.02, the bearing damping coefficient is 0.2 and the spring stiffness is 0.74. The unsteady Euler equations

are solved for locally-conical flows. The computational grid is of 64×64×2 in the wrap around, normal and axial directions, respectively. For these flow conditions, the steady flow is asymmetric, and hence $C_r \neq 0$ at $t = 0$. Therefore, we set $\theta_1^o = \dot{\theta}_1^o = 0$. The Euler equations of fluid flow and of rigid-body dynamics are sequentially integrated accurately in time with $\Delta t = 0.0025$. Figures 2 and 3 show the results of this case. Figure 2 shows the time responses of θ_1, C_r and C_a and the corresponding phase planes of $\dot{\theta}_1$ vz θ_1, C_r vz θ_1 and C_a vz θ_1. The time responses show the long time, $t \simeq 7$, it takes to build up the growing roll-angle response. The responses clearly show that the θ_1 and C_r continuously increase in time with increasing frequencies. The limit-cycle response is reached at $t \simeq 21$ which is clearly shown on the phase planes. The mean amplitude of θ_1 is –0.5°, its maximum is 40° and its minimum is –41°. Figure 3 shows snap shots of the surface-pressure coefficient and cross-flow velocity at the instants corresponding to points 1 and 2 on Fig. 2. The strong asymmetric motion of the primary vortices are clearly seen. Also, the surface-pressure-coefficient response clearly shows the generation of the restoring rolling moment to the wing motion.

Active Control of Wing Rock Using Leading-Edge Flaps Oscillation

The next step is to control the wing rock response of the previous case. For this purpose a leading-edge flap hinge is assumed to be at the 76% location of the local-half-span length. The flaps motion is introduced at $t_o = 13.02$ when $\theta_1 = -4°$ and $C_r = 0.0$. The flaps motion is anti-symmetric and is given by $\theta_{21}(t) = \theta_{21\,max} \sin k_f(t - t_o)$, where k_f is the flap reduced frequency. With the aid of the previous values of θ_1, C_r and k of the wing (can be measured by sensors to feed back the leading-edge flaps motion), we chose $\theta_{21\,max} = -0.5°$ and $k_f = 6.7$. Equation (15) for the wing-flaps motion is sequentially integrated accurately in time, with $\Delta t = 0.0025$, along with the Euler equations of fluid flow, and the ND equation is used for the grid deformation. Figure 4 shows the time responses of θ_1 and C_r for the wing. It is clearly seen that θ_1 response is damped within $t - t_o = 13$ with a mean value of 5°. However, the wing is still oscillating periodically around this mean position with a small amplitude. Next, the flaps motion is modified by dividing the amplitude $\theta_{21\,max}$ by $1 + (t - t_o)$ so that it decays with time. Figure 5 shows the steady response of the wing at $t = 30$. The wing assumes an equilibrium position of 5° without any oscillation. To check that this is a stable equilibrium position, the wing is disturbed at $t = 40$ with a small $\dot{\theta}_1$. Figure 5 also shows the time responses of θ_1 and C_r after the disturbance confirming that the equilibrium position is stable. Figure 6 shows the phase planes of the whole response history of θ_1 and C_r. Figures 7–9 show the same results as those of Figs. 4–6 when the same control is applied at $t_o = 23.27$, which is during the limit cycle response.

4

Simulation of Wing-Rock Motion (Three-Dimensional Flow)

Next, we consider the three-dimensional-flow simulation of the wing-rock problem.

A sharp-edged delta wing with a leading-edge sweep of 80° is considered for the computational applications. The angle of attack is set at 30° and the freestream Mach number is chosen as 0.3 for low speed simulation. The wing mass-moment of inertia about its axis is 0.285, the bearings damping coefficient is 0.15 and the torsional springs stiffness is 0.74. The unsteady Euler equations are solved for the three-dimensional flows. The boundary of the computational domain consists of a hemispherical surface with it center at the wing trailing edge on its line of geometric symmetry. The hemispherical surface is connected to a cylindrical aftersurface with its axis coinciding with the wing axis. The hemispherical and cylindrical radii are two root-chord lengths and the downstream, circular exit boundary is at two root-chord lengths from the wing trailing edge. The grid consists of $48 \times 32 \times 32$ grid points in the wrap-around, normal and axial directions, respectively. The grid is generated in the crossflow planes using a modified Joukowski transformation, which is applied at the grid-chord stations with exponential clustering at the wing surface.

Since the steady flow solution is asymmetric, C_r in Eq. (16) is of non-zero value and hence Eq. (16) is initially inhomogeneous. At $t = 0$, we set $\theta^o = \dot{\theta}^o = 0$ and release the wing with its initial M_s value as the driving rolling moment. At $t = \Delta t$, Eq. (16) of the wing dynamics is integrated to obtain θ_1 and hence $\dot{\theta}_1$ and $\ddot{\theta}_1$ ($\Delta t = 0.005$). Then, Eqs. (1-11) of the fluid flow are integrated to obtain the components of the flowfield vector and hence p and C_r. Next, t is increased to $2\Delta t$ and the sequential integration of the dynamics equation and the fluid flow equations is repeated. The sequential solutions are repeated until the limit-cycle amplitude response is reached

In Fig. 10, we show the roll angle, rolling-moment coefficient, C_r, and normal-force coefficient, C_n, versus time. Significant transient responses develop in the time range of $t = 0 \rightarrow 22$, wherein the amplitudes of the responses increase and decrease. Thereafter, $t > 22$, the amplitudes of the responses continuously increase until $t = 95$. At $t \geq 95$, the amplitudes and frequencies of the responses become periodic reaching the limit-cycle response. During the limit-cycle response, the maximum roll angle, θ_{1max}, is 10°, the minimum roll angle, θ_{1min}, is −11° and the period of oscillation is 3.53, which corresponds to a frequency of 1.78. With $\Delta t = 0.005$, each cycle of oscillation in the limit-cycle response requires 706 time steps. The shown responses, up to $t = 140$, required 28,000 time steps.

Next, we consider one cycle of the limit-cycle response and analyze the roll angle, rolling-moment-coefficient and normal-force-coefficient responses to gain physical insight of the wing-rock phenomenon. For this purpose, we show in Fig. 11 θ_1, C_r and C_n vz. t in the range of $t = 135.19 \rightarrow 138.72$. This period of oscillation is marked by the numbers 1, 2, 3, 4 and 5 in Fig. 11. In the first quarter of the cycle (1 → 2), the roll angle of the left side of the wing decreases from 0° → −11° and the wing rolls in the clockwise (CW) direction, the rolling-moment coefficient increases and changes sign from −0.057 → 0.0 → + 0.023 and the normal-force coefficient decreases and then increases from 2.68 → 2.65 → 2.75. It is important to notice that the rolling moment changes its sign which means that the rolling moment during the first part of this quarter of the cycle is in the CW direction (the same direction as the motion) and in the second part of this quarter of the cycle is in the CCW direction (the opposite direction of the motion). Hence, the rolling moment increases the negative angle in the first part and then it limits the growth of the roll angle in the second part. In the second quarter of the cycle (2 → 3) the roll angle increases from −11° → 0 and the wing rolls in the CCW direction, the rolling-moment coefficient increases and then decreases from +0.023 → 0.045 → 0.04 and the normal-force coefficients increases and then decreases from 2.75 → 3.0 → 2.84. The rolling-moment coefficient is in the CCW direction (the same direction as the motion). In the third quarter of the cycle (3→4) the roll angle increases from 0 → 10° and the wing keeps its rolling motion in the CCW direction, the rolling-moment coefficient decreases and changes sign from +0.04 → 0 → −0.038 and the normal-force coefficient decreases and then increases from 2.84 → 2.78 → 2.86. Again, it is noticed that the rolling moment changes its sign from CCW to CW directions and limits the roll angle growth.

In Figs. 12 and 13, we show snapshots at points 2 and 4, respectively; of the cross-flow-velocity vectors and the static-pressure contours at the chord stations of 0.54, 0.63 and 0.79 and the surface-pressure coefficient at the chord stations of 0.54 and 0.63. In Fig. 12, the primary vortex on the right side is nearer to the upper wing surface than the one on the left side. Moreover, the primary vortex on the right is further away from the plane of geometric symmetry in comparison to the one on the left. The surface-pressure curves show large peaks on the right side and that the surface-pressure difference on the right side is larger than the one on the left side. This results into a CCW rolling moment at this maximum negative roll angle of −11°. In Fig. 13, the opposite process occurs; the surface-pressure difference on the left side is larger than the one on the right side and this results into a CW rolling moment at this maximum positive roll angle of +10°. These results are consistent with those of the experimental data of Refs. 3 and 4.

In Fig. 14, we show the variations of the maximum static pressure of the vortex cores of the primary vortices

on the left and right sides versus the roll angle for the chord station of 0.54. The numbers on the figures correspond to those in Fig. 11. Since the maximum static pressure of the core is proportional to the vortex-core strength, it is obviously seen that the primary vortex on the right side has a greater strength at point 2 as compared to that on the left side. The strength differential between the right and left vortices along with the locations of the vortex cores contributes substantially to the net total CCW rolling moment which limits the negative growth of the roll angle and reverses the wing motion. Similarly, it is concluded that the strength differential between the left and right vortices at point 4 substantially contributes to the net total CW rolling moment which limits the positive growth of the roll angle and reverses the wing motion.

In Fig. 15, we split the rolling-moment coefficient into restoring and damping components similar to Konstadinopoulos, et al.[9]. First, the rolling-moment coefficient C_r is fitted using the following expansions in terms of θ and $\dot{\theta}$:

$$
\begin{aligned}
C_r = {} & a_1\theta + a_2\dot{\theta} + a_3\theta^3 + a_4\theta^2\dot{\theta} \\
& + a_5\dot{\theta}^2\theta + a_6\dot{\theta}^3 + a_7\theta^3 + a_8\theta^4\dot{\theta} \\
& + a_9\theta^2\dot{\theta}^3 + a_{10}\dot{\theta}^2\theta^3 + a_{11}\dot{\theta}^4\theta + a_{12}\dot{\theta}^5 \quad (17)
\end{aligned}
$$

The coefficients $a_1 - a_{12}$ are determined using a least-squares fit. A comparison of the original (-⊕-) and fitted (-✕-) rolling-moment coefficients is shown in Fig. 15. Next, we split the fitted-rolling-moment coefficient into a restoring part, M_r, and a damping part, M_d, as follows:

$$
\begin{aligned}
M_r = {} & \left(a_1 + a_5\dot{\theta}^2 + a_{11}\dot{\theta}^4\right)\theta \\
& + \left(a_3 + a_{10}\dot{\theta}^2\right)\theta^3 + a_7\theta^5 \quad (18)
\end{aligned}
$$

$$
\begin{aligned}
M_d = {} & \left(a_2 + a_4\theta^2 + a_8\theta^4\right)\dot{\theta} \\
& + \left(a_6 + a_9\theta^2\right)\dot{\theta}^3 + a_{12}\dot{\theta}^5 \quad (19)
\end{aligned}
$$

In Fig. 15, we also show M_r and θ versus time, and M_d and θ versus time. Moreover, we show on these figures the numbers 1, 2, 3, 4 and 5 which correspond to the same numbers in Figs. 11 and 14. In the first quarter of the cycle (1→2), the roll angle θ decreases from $0 \rightarrow -11°$, the restoring rolling moment becomes negative during the first part and positive during the second part and the damping rolling moment, which is negative at point 1, increases during the first part and becomes almost zero during the second part. It is very interesting to notice that M_r and M_d are negative during the first part and hence they are in the same direction as the motion. During the second part, M_r becomes positive reaching its maximum at point 2 when $\theta_{max} = -11°$ and hence it limits the angle growth. During the same second part, M_d becomes almost zero indicating a loss of damping rolling moment. In the second quarter

of the cycle (2→3), M_r stays almost constant during the first part and drops to zero in the second part when the roll angle becomes $0°$. During the same second quarter, M_d continuously increases from 0 to a maximum positive value when the roll angle becomes 0. In the third quarter of the cycle (3-4), a similar interaction of θ, M_r and M_d as that of the first quarter (1-2) occurs except with opposite signs. These conclusions are exactly similar to those of Ref. 9. Hence, the loss of damping rolling moment is responsible for the wing-rock motion.

CONCLUDING REMARKS

The multidisciplinary problem of wing-rock motion and its active control has been simulated using the unsteady, compressible, Euler equations; the Euler equation of rigid-body dynamiocs and the ND equations for the grid deformation. The fluid flow Euler equations are solved using an implicit, approximately factored, central-difference, finite-volume scheme; rigid-body Euler equation is solved using a four-stage, Runge-Kutta scheme and the ND equations are solved using an ADI scheme. Simulation of the wing-rock problem is obtained for a delta wing which is mounted on an axle with torsional springs and the axle is free to rotate in bearings with viscous damping. The wing starts its motion under the effect of an initial rolling moment due to the initially asymmetric flow at zero roll angle and zero angular velocity. For the active control of wing-rock motion, a tuned anti-symmetric leading-edge flaps oscillation is used to achieve that purpose. Also, it has been shown that the hysteresis responses of position and strength of the asymmetric right and left primary vortices are responsible for the wing rock motion. Moreover, it has also been shown that the loss of aerodynamic damping rolling moment at the zero angular velocity value is a main reason for the wing rock motion. These conclusions are consistent with the previous findings of the experimental[3,4] and computational[9] research work.

REFERENCES

1. Nguyen, L. T., Yip, L. and Chambers, X., Jr., "Self-Induced Wing Rock of Slender Delta Wings," AIAA Paper No. 81-1883, August 1981.

2. Levin, D. and Katz, J., "Dynamic Load Measurements with Delta Wings Undergoing Self-Induced Roll-Oscillations," Journal of Aircraft, Vol. 21, January 1985, pp. 30-36.

3. Jun, Y. W. and Nelson, R. C., "Leading Edge Vortex Dynamics on a Delta Wing Undergoing a Wing Rock Motion," AIAA-87-0332, January 1987.

4. Arena, A. S., Jr. and Nelson, R. C., "The Effect of Asymmetric Vortex Wake Characteristics on a Slender Delta Wing Undergoing Wing Rock Motion," AIAA 89-3348-CP, August 1989, pp. 16-24.

5. Arena, A. S. and Nelson, R. C., " Unsteady Surface Pressure Measurements on a Slender Delta Wing Undergoing Limit Cycle Wing Rock," AIAA paper No. 91-0434, January 1991.

6. Morris, S. L. and Ward, D. T., "A Video-Based Experimental Investigation of Wing Rock," AIAA 89-3349-CP, August 1989, pp. 25-35.

7. Ericsson, L. E., "The Fluid Mechanics of Slender Wing Rock," Journal of Aircraft, Vol. 21, May 1984, pp. 322-328.

8. Ericsson, L. E., "Various Sources of Wing Rock," Journal of Aircraft, Vol. 27, June 1990, pp. 488-494.

9. Konstandinopoulos, P., Mook, D. T. and Nayfeh, A. H., "Subsonic Wing Rock of Slender Delta Wings," Journal of Aircraft, Vol. 22, March 1985, pp. 223-228.

10. Elzebda, J. M., Nayfeh, A. H. and Mook, D. T., "Development of an Analytical Model of Wing Rock for Slender Delta Wings," Journal of Aircraft, Vol. 26, August 1989, pp. 737-743.

11. Nayfeh, A. H., Elzebda, J. M. and Mook, D. T., "Analytical Study of the Subsonic Wing-Rock Phenomenon for Slender Delta Wings," Journal of Aircraft, Vol. 26, September 1989, pp. 805-809.

12. Hsu, C. and Lan, C. E., "Theory of Wing Rock," Journal of Aircraft, Vol. 22, Oct. 1985, pp. 920-924.

13. Kandil, O. A. and Chuang, H. A., "Computation of Steady and Unsteady Vortex Dominated Flows with Shock Waves," AIAA Journal, Vol. 26, No. 5, 1988, pp. 524–531.

14. Kandil, O. A. and Chuang, H. A., "Unsteady Transonic Airfoil Computation Using Implicit Euler Scheme on Body-Fixed Grid," AIAA Journal, Vol. 27, No. 8, August 1989, pp 1031-1037.

15. Kandil, O. A. and Chuang, H. A., "Unsteady Delta-Wing Flow Computation Using an Implicit Factored Euler Scheme," First National Fluid Dynamics Congress, July 1988. Also AIAA Journal, Vol. 28, No. 9, September 1990, pp. 1589-1595.

16. Kandil, O. A. and Chuang, H. A., "Unsteady Navier-Stokes Computations Past Oscillating Delta Wing at High Incidence," AIAA-89-0081, January 1989. Also AIAA Journal, Vol. 28, No. 9, September 1990, pp. 1565-1572.

17. Batina, J. T., "Vortex-Dominated Conical-Flow Computations Using Unstructured Adaptively-Refined Meshes," AIAA Journal, Vol. 28, No. 11, Nov. 1990, pp. 1925-1932.

18. Lee, E. M. and Batina, J. T., "Conical Methodology for Unsteady Vortical Flows about Rolling Delta Wings," AIAA-91-0730, January 1991.

19. Kandil, O. A. and Salman, A. A., "Unsteady Vortex-Dominated Flow Around Wings with Oscillating Leading-Edge Flaps," AIAA 91-0435, January 1991.

20. Kandil, O. A. and Salman, A. A., "Unsteady Supersonic Flow Around Delta Wings with Symmetric and Asymmetric Flaps Oscillation," AIAA 91-1105-CP, April 1991, Vol. 3, pp. 1888-1903.

21. Kandil, O. A. and Salman, A. A., "Effect of Leading-Edge Flap Oscillation on Unsteady Delta Wing Flow and Rock Control," AIAA-91-1796, June 1991.

22. Kandil, O. A. and Salman, A. A., "Recent Advances in Unsteady Computations and Applications of Vortex Dominated Flows," Invited paper, 4th International Symposium on Computational Fluid Dynamics, University of California, Davis, September 9-12, 1991, pp. 570-575.

23. Kandil, O. A. and Salman, A. A., "Three-Dimensional Simulation of Slender Delta Wing Rock and Divergence," AIAA 92-0280, January 1992.
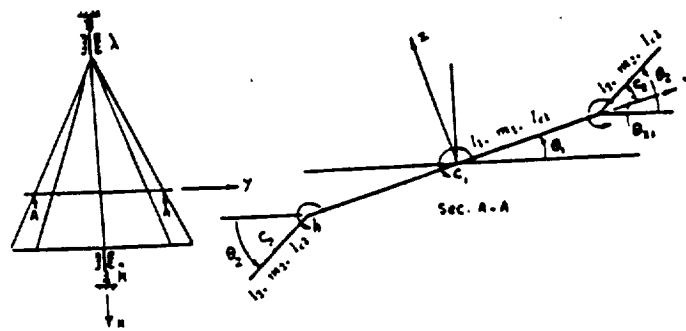
Fig. 1 Wing-Flaps Dynamics for Rolling Motion.
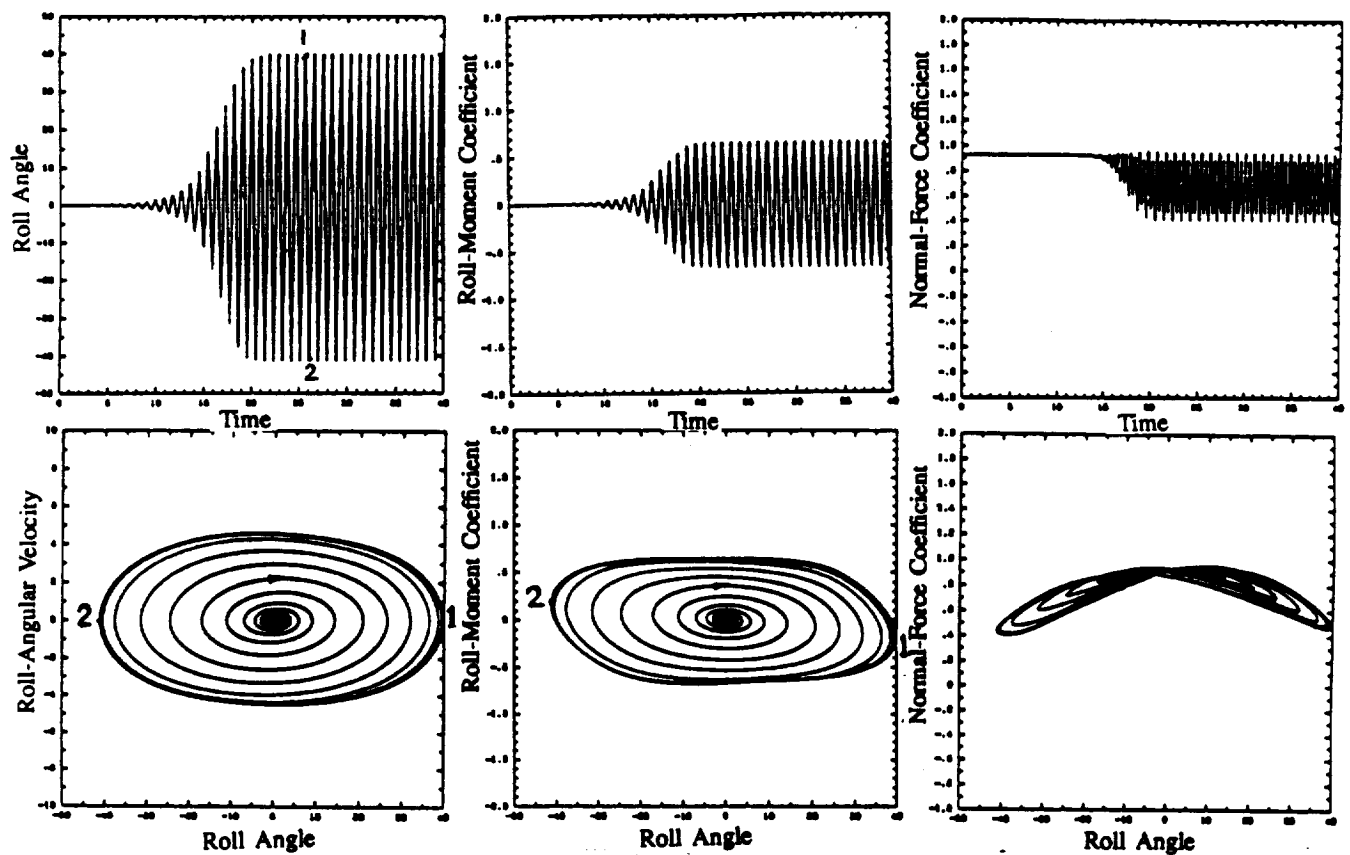
Fig. 2 Roll-Angle, Roll-Moment-Coefficient and Normal-Force-Coefficient Responses for an Unstable Rolling Motion (Wing Rock), $\beta = 80°$, $\alpha = 35°$, $M_\infty = 1.4$, $I_{xx} = 0.02$, $\lambda = 0.$, $\hat{k} = 0.74$, $\Delta t = 0.0025$, $\theta_1^o = \dot{\theta}_1^o = 0$.
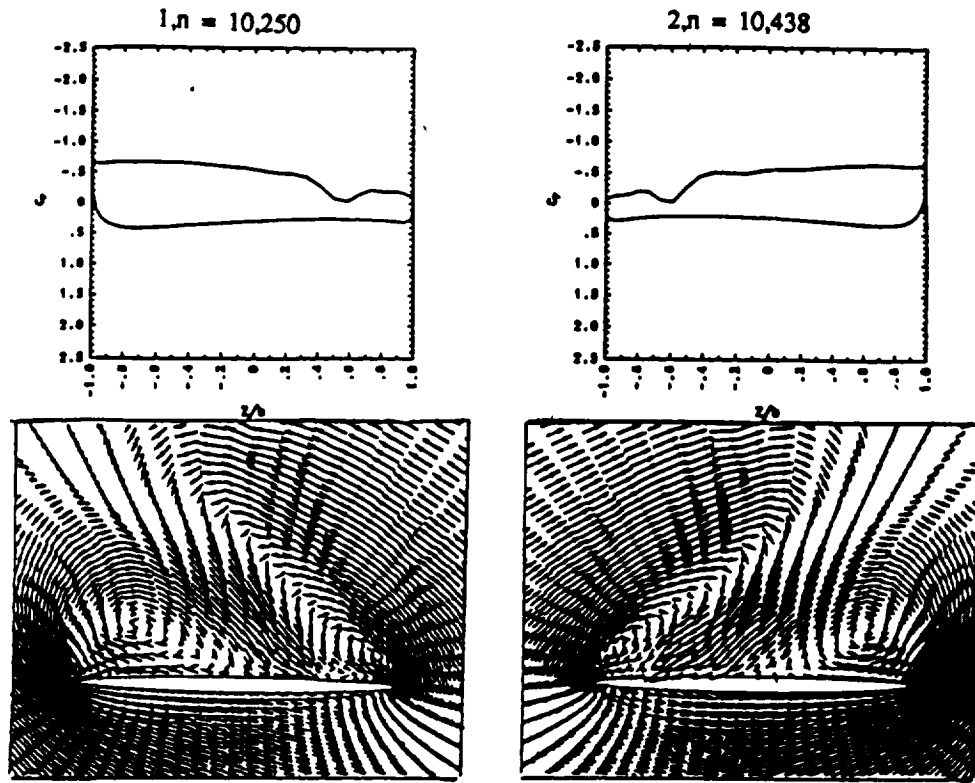
Fig. 3 Surface-Pressure Coefficient and Cross-Flow Velocity During the Limit-Cycle Response, $\beta = 80°$, $\alpha = 35°$, $M_\infty = 1.4$, $\Gamma_{xx} = 0.02$, $\lambda = 0.$, $\hat{k} = 0.74$, $\Delta t = 0.0025$, $\theta_1^o = \dot{\theta}_1^o = 0$.
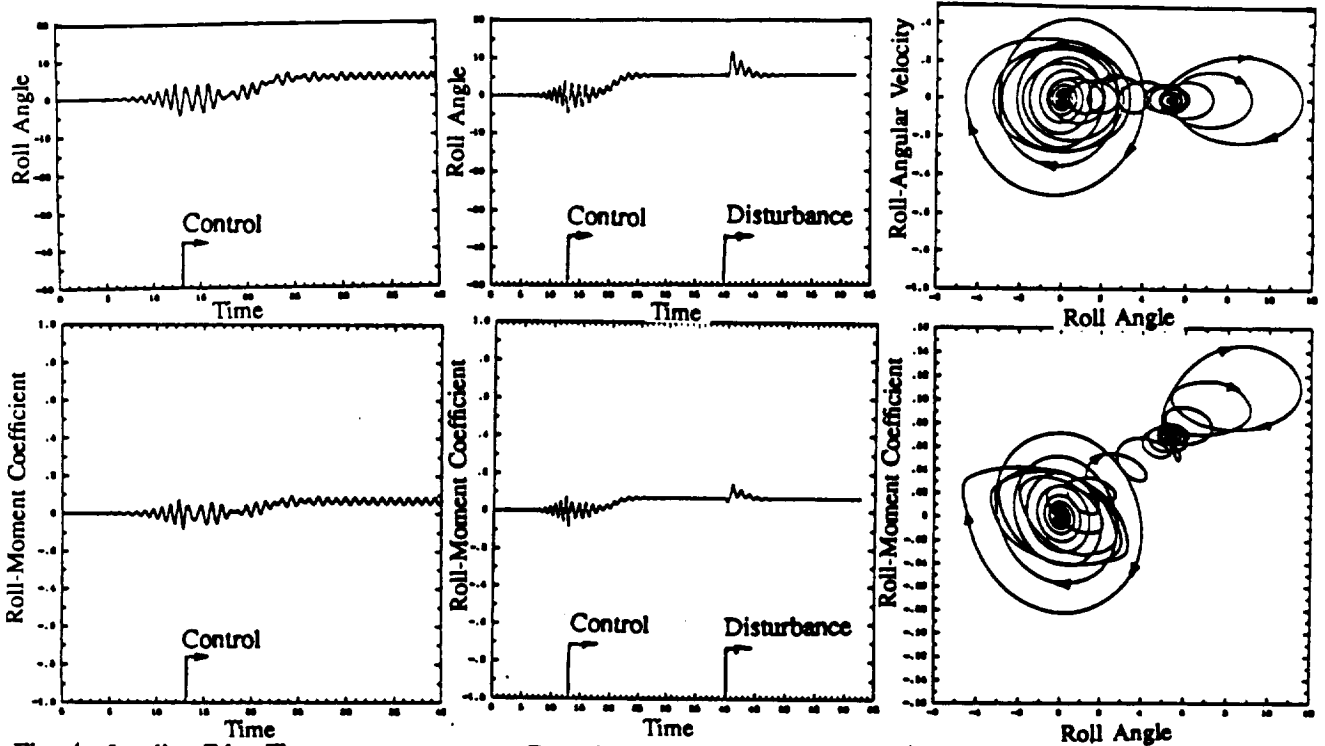
Fig. 4 Leading-Edge Flaps Active Control, $\theta_{21} = \theta_{21\,max} \sin k_f(t - t_o)$, $\alpha = 35°$, $M_\infty = 1.4$, $t_o = 13.02$

Fig. 5 Decaying-amplitude active control followed by disturbance, $\theta_{21} = \frac{\theta_{21\,max}}{1+(t-t_o)} \sin k_f(t - t_o)$, $\alpha = 35°$, $M_\infty = 1.4$, $t_o = 13.02$

Fig. 6 Phase Planes Covering History of Responses; Instability, Control and Disturbance, $\alpha = 35°$, $M_\infty = 1.4$, $t_o = 13.02$
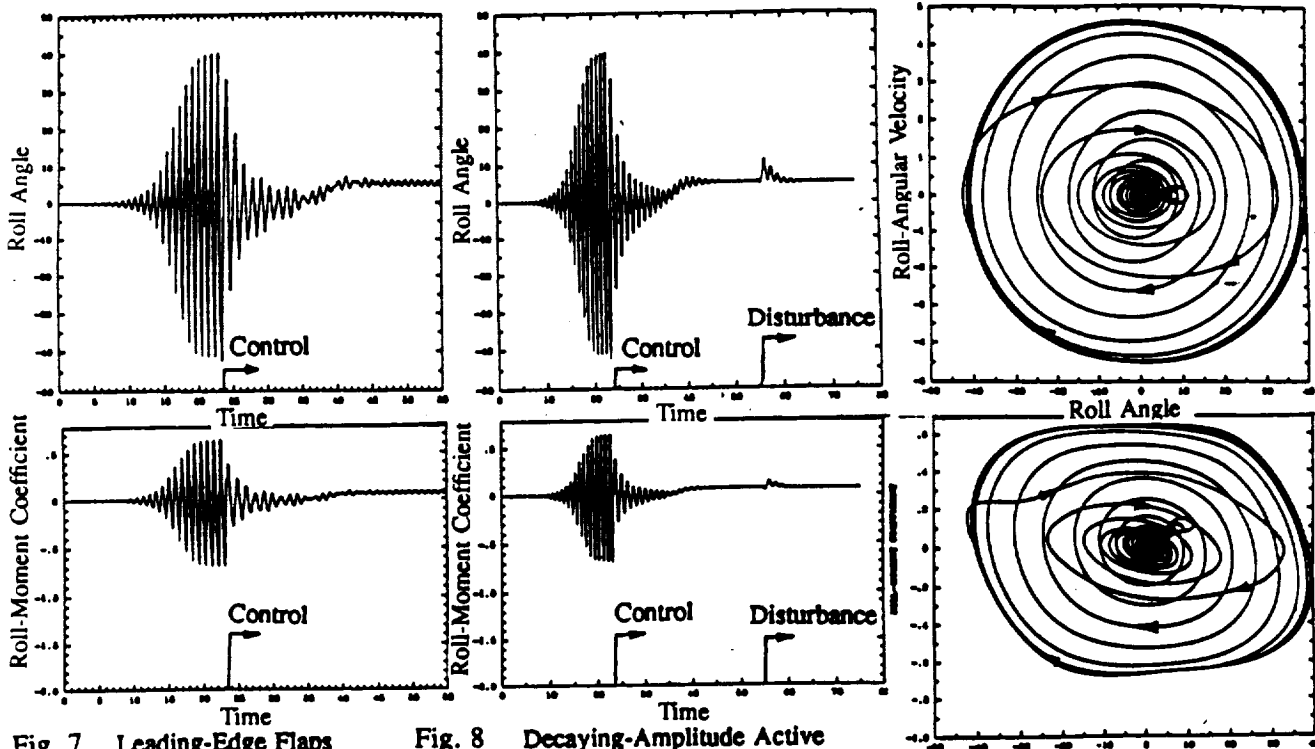
Fig. 7   Leading-Edge Flaps
         Active Control,
         $\theta_{21} = \theta_{21\,max} \sin k_f(t - t_o)$,
         $\alpha = 35°$, $M_\infty = 1.4$, $t_o = 23.7$

Fig. 8   Decaying-Amplitude Active
         Control Followed by Disturbance,
         $\theta_{21} = \frac{\theta_{21\,max}}{1+(t-t_o)} \sin k_f(t - t_o)$,
         $\alpha = 35°$, $M_\infty = 1.4$, $t_o = 23.7$

Fig. 9   Phase Planes Covering History
         of Response: Instability,
         Control and Disturbance,
         $\alpha = 35°$, $M_\infty = 1.4$, $t_o = 23.7$
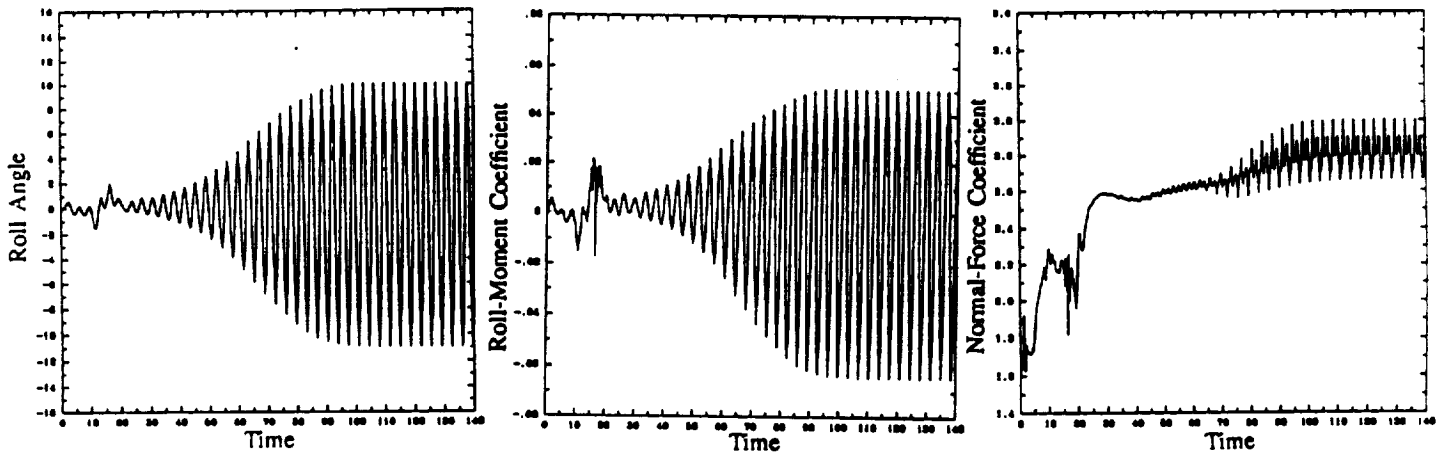
Fig. 10. Roll angle, roll-moment-coefficient and normal-force-coefficient response
          for wing-rock motion; delta wing, $\alpha = 30°$, $M_\infty = 0.3$, $I_{xx} = 0.285$, $\lambda = 0.15$, $\hat{k} = 0.74$, $\theta_1^\bullet = \dot{\theta}_1^\bullet = 0$.
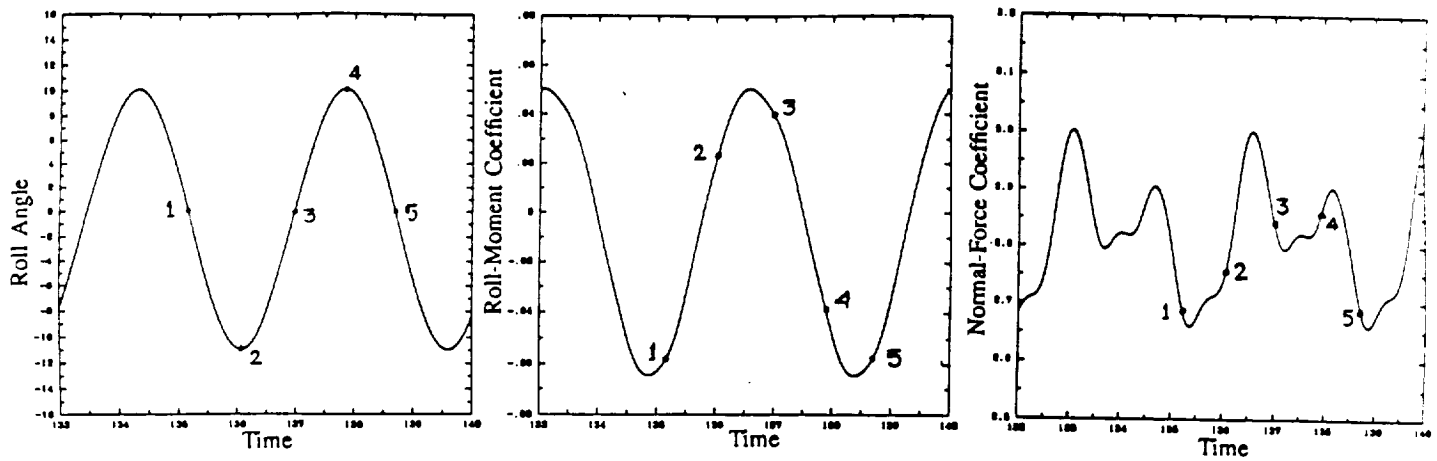
Fig. 11. Time responses for wing-rock motion during the limit cycle response.
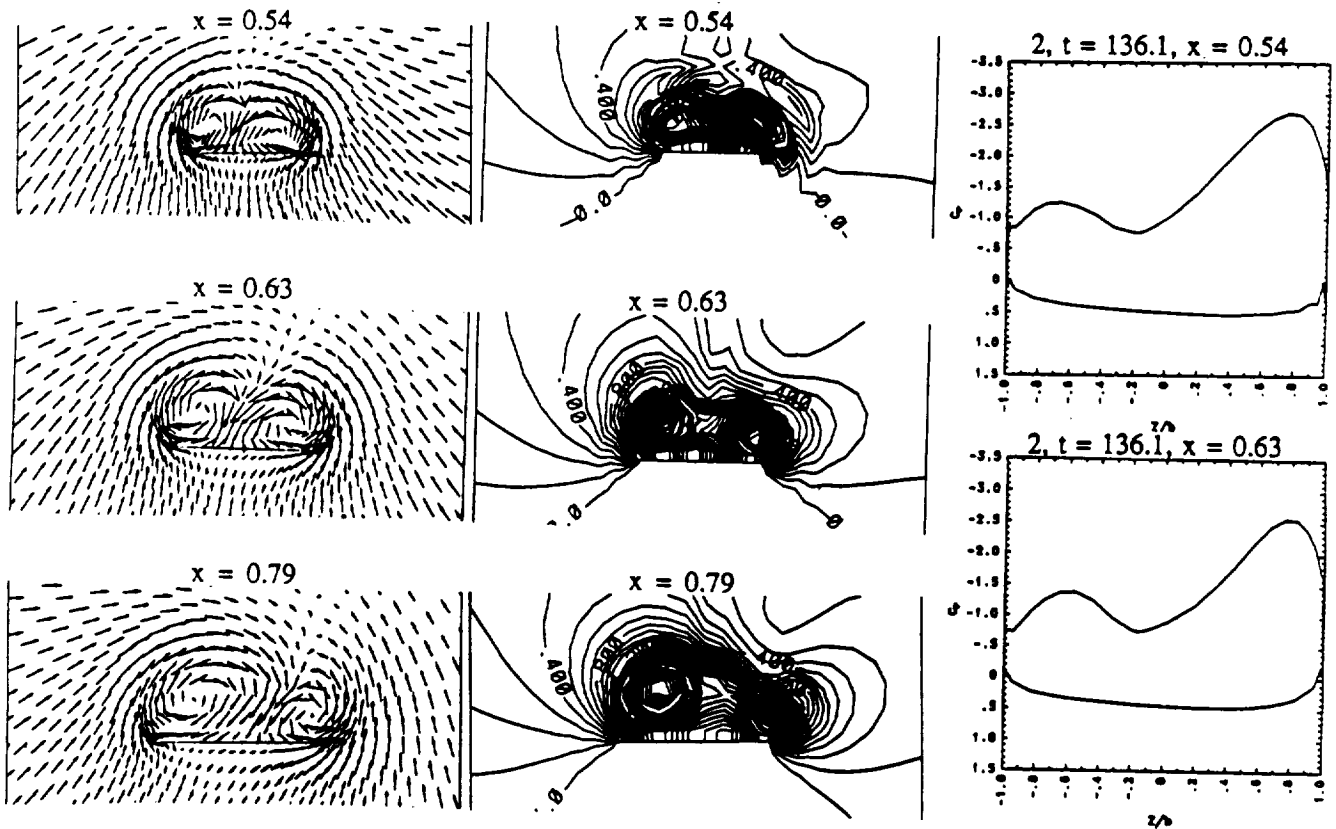
Fig. 12. Snapshot at point 2 of crossflow velocity, static-pressure contours and surface pressure for wing-rock motion.
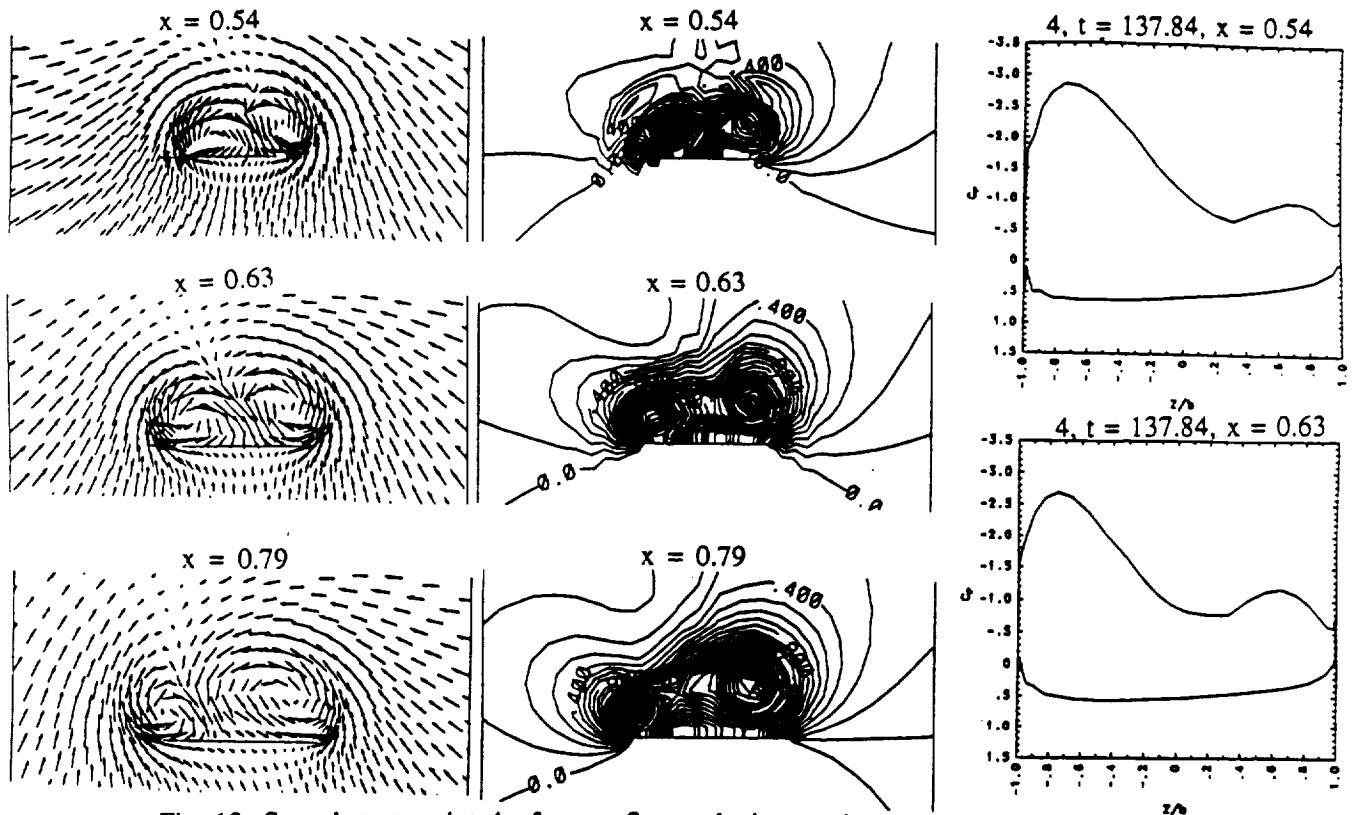
Fig. 13. Snapshot at point 4 of cross flow velocity, static-pressure contours and surface pressure for wing-rock motion.
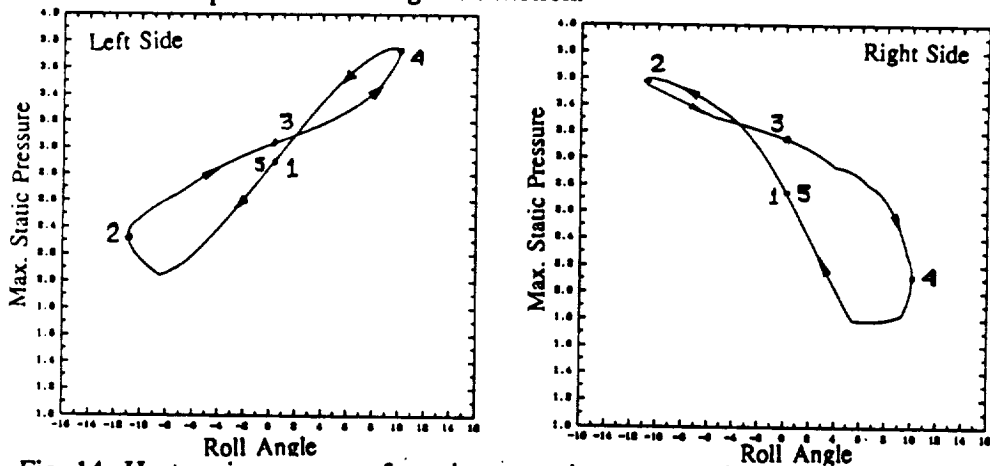
Fig. 14. Hysteresis response of maximum static pressure of right and left primary vortices for wing-rock motion during the limit-cycle response.
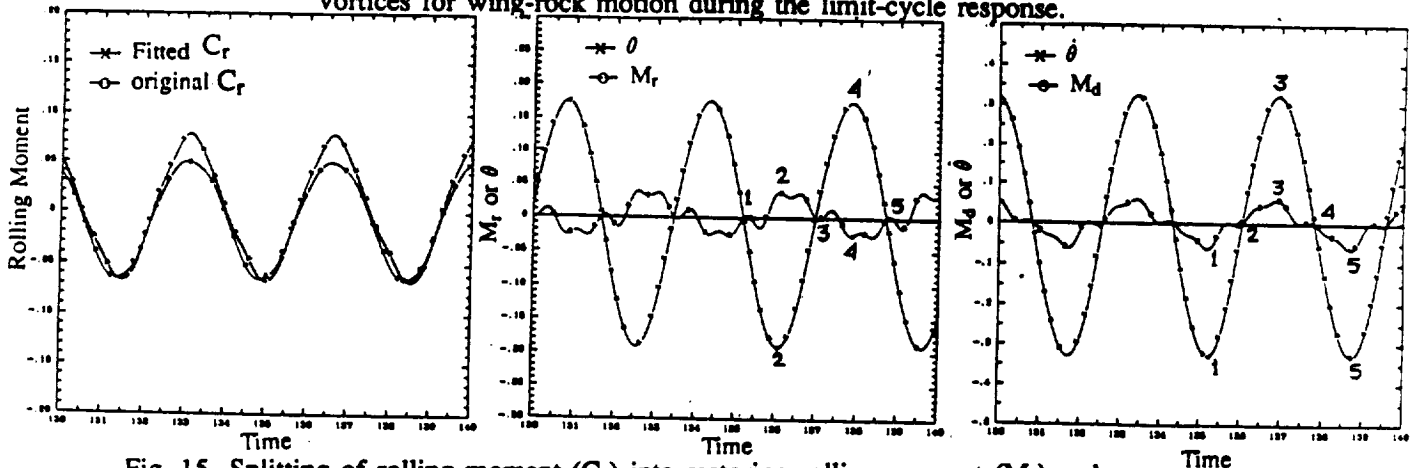
Fig. 15. Splitting of rolling moment (C_r) into restoring rolling moment (M_r) and damping rolling moment (M_d) for wing-rock motion during the limit-cycle response.

UNSTEADY EULER AND NAVIER-STOKES COMPUTATIONS AROUND OSCILLATING DELTA WING INCLUDING DYNAMICS

by

Ahmed Abd-El-Bar Ahmed Salman

B. Sc., July 1977, Ain Shams University, Cairo, EGYPT

M. Sc., July 1984, Ain Shams University, Cairo, EGYPT
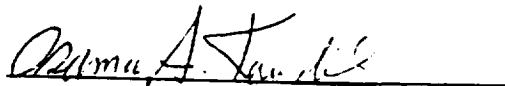
A Dissertation Submitted to the Faculty of
Old Dominion University in Partial Fulfillment of
the Requirements for the Degree of

DOCTOR OF PHILOSOPHY
MECHANICAL ENGINEERING

OLD DOMINION UNIVERSITY
April 1992

Approved by:

_____
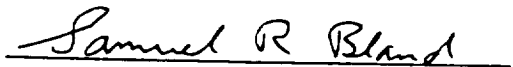
Osama A. Kandil (Director)

_____
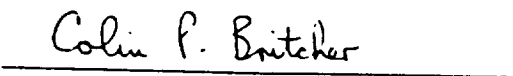
Robert L. Ash

_____

Woodrow Whitlow, Jr. (NASA LaRC)

_____

Samuel R. Bland   (NASA LaRC)

_____

Colin P. Britcher

Abstract

Unsteady Euler and Navier-Stokes Computations Around Oscillating Delta Wings Including Dynamics

Ahmed Abd-El-Bar Ahmed Salman
Old Dominion University, 1992

Director: Professor Osama A. Kandil

Unsteady flows around rigid or flexible delta wings with and without oscillating leading-edge flaps are considered. These unsteady flow problems are categorized under two classes of problems. In the first class, the wing motion is prescribed a priori and in the second class, the wing motion is obtained as a part of the solution. The formulation of the first class includes either the unsteady Euler or unsteady Navier-Stokes equations for the fluid dynamics and the unsteady linearized Navier-displacement equations for the grid deformation. For the formulation of the second class, the rigid-body dynamics equations are used, in addition to the fluid dynamics and grid-deformation equations, to obtain the wing motion.

Different computational schemes have been used to solve these equations. For the fluid-dynamics equations, an implicit, approximately-factored, central-differenced finite-volume scheme is used. For the rigid-body dynamics equation, an explicit, four-stage Runge-Kutta, time-stepping scheme is used. For the grid deformation equations, an alternating direction implicit (ADI) scheme is used. A modified Joukowski Transformation is used to generate conical and three-dimensional grids, and an elliptic grid generator is used to generate the two-dimensional grids.

The problem of unsteady transonic flow past a bicircular-arc airfoil undergoing prescribed thickening-thinning oscillation is studied using the CFL2D code. This code is used to solve the Navier-Stokes equations using an implicit, flux-difference splitting, finite-volume scheme. The unsteady linearized Navier-displacement (ND) equations are used to compute grid deformation. This application falls under the first class of problems described above. It demonstrates the validity of applying the developed schemes for flexible airfoils, by comparing present results with the available computational results.

For the unsteady supersonic flows around flexible delta wings with prescribed oscillating deformation and rigid delta wings with leading-edge-flap oscillations, the conservative, unsteady Euler and thin-layer Navier-Stokes equations in a moving frame-of-reference, along with the linearized ND equations, have been used. These problems are solved under the locally-conical flow assumption which substantially reduces the computational cost and still provides physical understanding of the flow behavior. Two main problems are solved to demonstrate the validity of the developed schemes. The first problem is that of a flexible delta wing undergoing a prescribed bending-mode oscillation. In the second problem, a rigid-delta wing with symmetric and anti-symmetric flap oscillations is considered. For the second problem, a parametric study of the effects of reduced frequency and hinge location is considered. The wing-flap problem also has been studied for different angles of attack and Mach numbers where shock waves could be either under or above the primary vortex of the leading-edge flaps. These applications fall under the first class of problems.

For the unsteady flow applications, where the wing motion is not prescribed a priori (second class of problems), either the unsteady Euler or thin-layer Navier-Stokes equations and the rigid-body dynamics equations, in a moving frame of reference, are solved sequentially to obtain the flow behavior and the wing motion. The main application for this class of unsteady flow phenomena, is the wing-rock problem. Using the locally-conical flow assumption, three problems are solved. The first is that of a delta wing undergoing a

damped rolling oscillation. The second is that of a delta wing undergoing a limit-cycle, wing-rock motion. In the third problem, suppression of the wing-rock motion is demonstrated using a tuned anti-symmetric oscillation of the leading-edge flaps. In the third problem, the unsteady linearized Navier-displacement equations are also used to account for the grid deformation due to the leading-edge flap motion.

Next, the locally-conical-flow assumption has been relaxed and the unsteady, three-dimensional, subsonic flow around a sharp-edged delta wing undergoing a limit-cycle wing-rock motion has been solved. For this problem, the unsteady Euler equations are solved sequentially along with the rigid-body dynamics equation.

ACKNOWLEDGMENTS

Table of Contents

v